J Comput Aided Mol Des (2016) 30:489–512
DOI 10.1007/s10822-016-9919-y

Molecular dynamics simulations and structure-based network analysis reveal structural and functional aspects of G-protein coupled receptor dimer interactions

Fotis A. Baltoumas[1] · Margarita C. Theodoropoulou[1,2] · Stavros J. Hamodrakas[1]

Received: 27 January 2016 / Accepted: 22 June 2016 / Published online: 27 June 2016

Abstract A significant amount of experimental evidence suggests that G-protein coupled receptors (GPCRs) do not act exclusively as monomers but also form biologically relevant dimers and oligomers. However, the structural determinants, stoichiometry and functional importance of GPCR oligomerization remain topics of intense speculation. In this study we attempted to evaluate the nature and dynamics of GPCR oligomeric interactions. A representative set of GPCR homodimers were studied through Coarse-Grained Molecular Dynamics simulations, combined with interface analysis and concepts from network theory for the construction and analysis of dynamic structural networks. Our results highlight important structural determinants that seem to govern receptor dimer interactions. A conserved dynamic behavior was observed among different GPCRs, including receptors belonging in different GPCR classes. Specific GPCR regions were highlighted as the core of the interfaces. Finally, correlations of motion were observed between parts of the dimer interface and GPCR segments participating in ligand binding and receptor activation, suggesting the existence of mechanisms through which dimer formation may affect GPCR function. The results of this study can be used to drive experiments aimed at exploring GPCR oligomerization, as well as in the study of transmembrane protein–protein interactions in general.

Keywords G-protein coupled receptors · Oligomerization · Molecular dynamics · Network analysis

Introduction

G-protein coupled receptors (GPCRs) are one of the largest and most diverse superfamilies of membrane receptors in eukaryotic cells. They regulate the majority of cell responses to stimuli and have been implicated in a wide range of diseases, including neurological syndromes, cardiac diseases, HIV infection and various types of cancer [1]. As a result, today GPCRs are targets for more than 40 % of pharmaceuticals on the market [2]. Most GPCR functions are conducted through heterotrimeric G-proteins, composed by Gα subunits and Gβγ heterodimers which, in turn, regulate the function for a wide variety of effectors. However, a number of alternative signaling pathways, either complementary to the G-protein pathway or completely independent, have also been identified [1, 3].

GPCRs are usually grouped into six classes (A–F), four of which (namely A, B, C and F) are present in Metazoa [4]. GPCRs from all Classes share a common topology, comprised by an extracellular N-terminus, seven transmembrane (TM) α-helices connected by three intracellular (ICL) and three extracellular (ECL) loops and followed by an amphiphilic 8th helix (H8) and a cytoplasmic C-terminus [2]. This topology has been confirmed by the growing number of GPCR crystal structures, including important Class A GPCRs such as the photoreceptor Rhodopsin [5], β1AR and

Electronic supplementary material The online version of this article (doi:10.1007/s10822-016-9919-y) contains supplementary material, which is available to authorized users.

✉ Stavros J. Hamodrakas
shamodr@biol.uoa.gr

[1] Department of Cell Biology and Biophysics, Faculty of Biology, National and Kapodistrian University of Athens, Panepistimiopolis, 15701 Athens, Greece

[2] Present Address: Department of Computer Science and Biomedical Informatics, University of Central Greece, 35131 Lamia, Greece

β2AR adrenergic receptors [6, 7], the A2A adenosine receptor [8] and the entire opioid receptor subfamily [9–11], the Smoothened receptor from Class F [12], the CRF1R corticotropin release factor 1 and glucagon receptors from Class B [13, 14] and metabotropic glutamate receptors mGluR1 and mGluR5 from Class C [15, 16].

An emerging paradigm in GPCR research is the notion that receptors do not act exclusively as monomers, but also form functionally relevant dimers and oligomers [17]. Numerous biophysical and biochemical trials have demonstrated the spatial organization of GPCRs in higher order assemblies, both in vitro and in vivo [18, 19]. Dimer formation has been repeatedly shown to be obligatory for canonical receptor function in class C GPCRs [20], while receptors from other classes have also been shown to be functional both as monomers and as oligomers [18]. Furthermore, biological fingerprint experiments have shown that formation of homo- and heterodimers or oligomers may influence important aspects in GPCR signaling pathways, such as ligand binding affinity, receptor activation or internalization and interactions with heterotrimeric G-proteins [18]. Finally, a significant number of GPCR oligomers have been implicated in various pathological conditions such as schizophrenia, Parkinson's disease, drug addiction, heart failure and asthma [21] and, in many cases, receptor homo- and heterodimers are believed to be more suitable targets for the design of novel drugs than monomers [17, 22–24].

Despite the accumulating experimental evidence and the functional significance of oligomerization, the structural determinants of GPCR dimers and oligomers remain controversial. Cross-linking and mutagenesis studies for several GPCRs [25–30], as well as Atomic Force and Cryo-Electron Microscopy studies for Rhodopsin [31–33] have identified transmembrane segments TM1, TM4, TM5 and TM6 and the cytoplasmic H8 helix as potential participants in the dimer interface, while recently solved crystal structures display symmetric parallel homodimers with interfaces resembling the ones proposed by experiments and involving interactions between TM1, TM2 and H8 (TM1–TM2–H8 dimers), TM4 and TM5 (TM4–TM5 dimers) or TM5 and TM6 (TM5–TM6 dimers) [17] (Fig. 1). A number of bioinformatics and computational biology studies, including all-atom and Coarse-Grained Molecular Dynamics simulations, sequence-based interface predictions and co-evolution analyses have also investigated the formation and stability of the afore mentioned interfaces [34–40]. However, the functional relevance of these crystallographic dimers remains a subject of intense debate.

The goal of this study was to investigate and evaluate the structural nature and dynamics of GPCR oligomeric interactions, based on the available structural data. The dynamic nature of GPCR dimers and the dimer interface stoichiometry were explored through Coarse-Grained Molecular Dynamics (CG-MD) simulations in model membranes, followed by reconstruction in atomistic detail. Original crystallographic data and simulation results were analyzed for the identification of important interface hot spots. Simulation results were combined with concepts from network theory for the analysis of dynamic networks and the study of correlated motions between GPCR structural aspects. The results of this study can be used to drive theoretical and experimental trials in the study of GPCR oligomers, as well as in the study of transmembrane protein–protein interactions in general.

Materials and methods

Structural data collection and manipulation

A set of representative crystal structures, containing GPCRs in parallel homodimers, was compiled through extensive search in the literature and the Protein Data Bank (PDB) [41]. These structures were used as the input in Molecular Dynamics simulations, followed by interface analysis and classification. In cases where different PDB entries represented the same crystallographic dimers, the structure with the best possible quality was selected. In some cases, multiple structures were included for a specific receptor; these involved occasions where the structures contained either different receptor conformations or different dimer interfaces for the same receptor. In cases when the crystal interfaces were not part of the asymmetric unit but inferred biological assemblies, the dimers were generated using the Protein Interfaces, Structures and Assemblies (PISA) service through the PDBePISA server [42]. Where necessary, T4 Lysozyme or soluble cytochrome b562 coordinates and non-essential heteroatoms were removed and missing loop segments were reconstructed.

In addition to the crystallographic data, a number of theoretical models for GPCR dimers, based on existing structural evidence, were subjected to simulation and analysis. Specifically, a model of oligomerized Rhodopsin by *Liang and co-workers* [31, 32], based on restraints derived from Atomic-Force Microscopy (AFM) and Cryo-Electron Microscopy (Cryo-EM), was retrieved from the RCSB PDB Theoretical Model archive and included in the dataset. This model features two different interfaces for the Rhodopsin dimer; namely, a TM4–TM5 and a TM1–TM1 dimer. Finally, a number of putative GPCR dimers were constructed, featuring alternative dimer interfaces not appearing in crystal structures. Specifically, TM4–TM4 dimers were constructed for δOR, μOR and mGluR1 receptors. These models were designed to accommodate restraints from biochemical evidence [28, 43], but feature

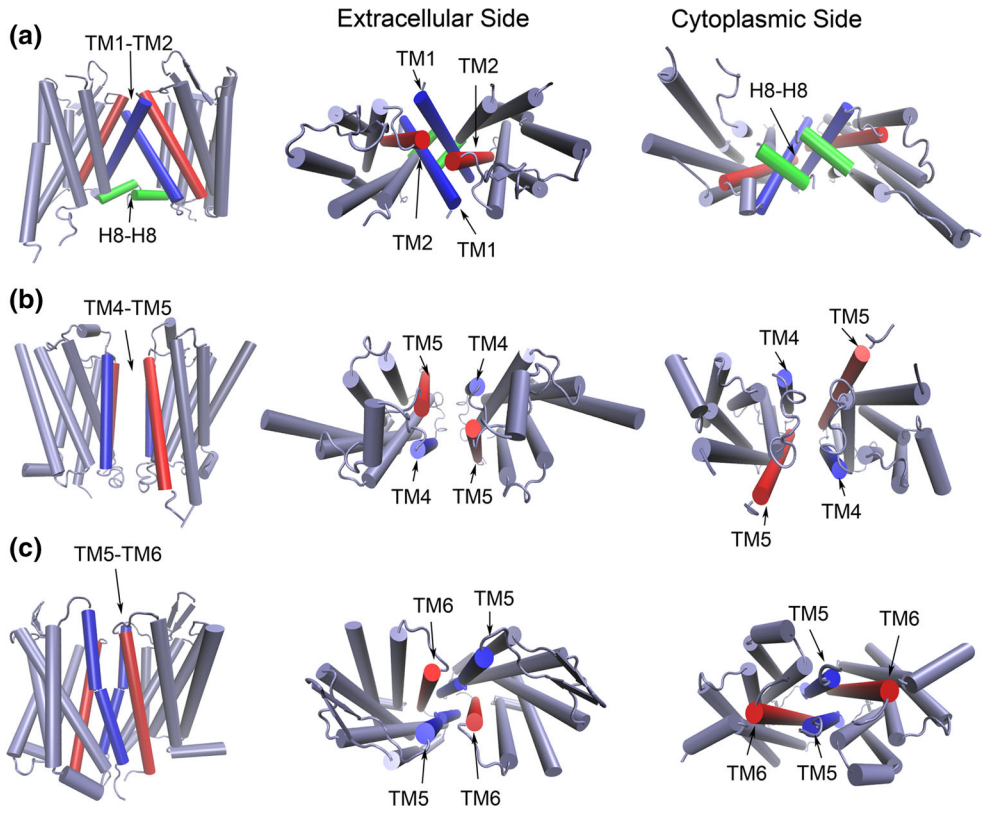

Fig. 1 Examples of commonly found GPCR crystallographic dimer interfaces. **a** The κ opioid receptor (κOR) TM1–TM2–H8 dimer. **b** The β1 adrenergic receptor (β1AR) TM4–TM5 dimer. **c** The μ opioid receptor (μOR) TM5–TM6 dimer. Helical segments are shown as cylinders, with interacting segments *colored blue*, *red* and *green*, while non-interacting segments are *colored grey*. The third intracellular loop (ICL3) loop segments are not shown for clarity

an alternative dimer interface that has been classified as energetically unfavorable, compared to the crystallographic dimers [36, 40]. Monomers from the mouse μOR, human δOR and mGluR1 crystal structures were used to construct the initial conformations. Where necessary, T4 coordinates and heteroatoms were removed and missing loop segments were reconstructed. The resulting models were used to build starting conformations, by manually positioning the protomers in configurations compatible with symmetric contacts of the TM4 or TM6 helices.

Manipulation, rendering and visualization of the structures were performed with PyMOL [44] and Visual Molecular Dynamics (VMD) [45]. Molecular modeling was performed using MODELLER v. 9.14 [46]. All relevant amino acid sequences were retrieved from UniProt [47] and alignments for modeling were performed using Clustal X v. 2.1 [48]. The final dataset of simulated GPCR dimers is presented in Tables 1 and 2 and Supplementary Table S1.

Coarse-grained molecular dynamics simulations

Coarse-Grained Molecular Dynamics simulations (CG-MD) were performed using the MARTINI Coarse-Grained force field and its extension to proteins [49, 50]. MARTINI utilizes a four to one mapping rule, meaning that, on average, four heavy atoms are represented by one Coarse-Grained particle. The accuracy and robustness of the force field has been validated for a number of biomolecules and processes, including the accurate reproduction of lipid bilayer properties such as the area per lipid, hydrophobic thickness and membrane curvature, the successful reproduction of dimerization free energy values obtained from all-atom simulations or thermodynamic data [49, 50] and simulations for several transmembrane proteins, including the study of Rhodopsin [34, 36] and adrenergic receptor homo-oligomerization [38, 51] and the hetero-oligomerization of opioid receptors [28, 39].

Each dimer was converted to Coarse-Grained (CG) representations using the MARTINI mapping scheme [52] and embedded in a lipid bilayer composed by 1-palmitoyl-2-oleyl-phosphatidyl-choline (POPC) phospholipids (Supplementary Figure S1). A special case was made for the cholesterol-containing β2AR and mGluR1 dimers, which were simulated with and without the original cholesterol molecules in a pure POPC membrane, as well as in a bilayer with a 9:1 POPC: cholesterol ratio [53]. A simple

Table 1 Overview of simulated GPCR crystallographic homodimers, including a brief description of the initial dimer interfaces and the changes observed during simulation

Receptor	PDB	Original dimer interface	Notes on the initial structure	Number of simulations[d]	Changes after simulation	Final dimer interface
Closely packed dimers						
Bovine Rhodopsin[a,b] (Class A)[c]	2I35	TM1–TM2–H8	The protomers form a ~20° angle between their principal axes	3 × 1 μs CG[d]	The angle between the protomers' principal axes is reduced; the dimer resembles κOR and β1AR	TM1–TM2–H8
Bovine Ligand-free Opsin[a] (Class A)	3CAP	TM1–TM2–H8	The protomers form a ~20° angle between their principal axes; different interface residues than 2I35	3 × 1 μs CG	The angle between the protomers' principal axes is reduced; the dimer resembles κOR and β1AR	TM1–TM2–H8
Human κ opioid receptor (κOR) (Class A)	4DJH	TM1–TM2–H8	Almost parallel protomers; extensive H8–H8 contacts	1 × 10 μs CG 3 × 1 μs CG	Very few changes are observed	TM1–TM2–H8
Mouse μ opioid receptor (μOR)[a,b] (Class A)	4DKL	TM1–TM2–H8	The protomers form a ~20° angle between their principal axes	3 × 1 μs CG	The angle between the protomers' principal axes is reduced; the dimer resembles κOR and β1AR	TM1–TM2–H8
Turkey β1 adrenergic receptor (β1AR) (Class A)	4GPO	TM1–TM2–H8	Almost parallel protomers	3 × 1 μs CG	Very few changes are observed	TM1–TM2–H8
Squid Rhodopsin[a,b] (Class A)	2Z73	TM4–TM5	Extensive TM4–TM5 contacts	3 × 1 μs CG	The inter-protomer distance is reduced	TM4–TM5
Human A2A adenosine receptor[b] (Class A)	4EIY	TM4–TM5	More loose interface compared to other TM4–TM5 dimers	3 × 1 μs CG	The inter-protomer distance is reduced	TM4–TM5
Turkey β1 adrenergic receptor (β1AR)[b] (Class A)	4GPO	TM4–TM5	More loose interface compared to other TM4–TM5 dimers	3 × 1 μs CG	The inter-protomer distance is reduced	TM4–TM5
Human Smoothened receptor (Class F)	4JKV	TM4–TM5	Extensive TM4–TM5 contacts	3 × 1 μs CG	Very few changes are observed	TM4–TM5
Human CXCR4 (Ligand: It1t)[a] (Class A)	3ODU	TM5–TM6	Loose TM5–TM6 contacts; T4 Lysozymes form part of the interface	1 × 10 μs CG 3 × 1 μs CG	The dimer adopts a TM4–TM5 orientation	TM4–TM5
Human CXCR4 (Ligand: CVX15)[a,b] (Class A)	3OE0	TM4–TM5–TM6	Loose TM5–TM6 contacts; T4 Lysozymes form part of the interface	3 × 1 μs CG	The dimer adopts a TM4–TM5 orientation	TM4–TM5
Mouse μ opioid receptor (μOR)[b] (Class A)	4DKL	TM5–TM6	Extensive TM5–TM6 contacts; T4 Lysozymes form part of the interface	1 × 10 μs CG 3 × 1 μs CG	Very few changes are observed	TM5–TM6

Table 1 continued

Receptor	PDB	Original dimer interface	Notes on the initial structure	Number of simulations[d]	Changes after simulation	Final dimer interface
Loosely packed dimers						
Squid Rhodopsin[a,b] (Class A)	2Z73	TM5–TM5	A loose interface in the cytoplasmic side of TM5	3 × 1 μs CG	The dimer adopts a TM5–TM6 orientation	TM5–TM6
Human β2 adrenergic receptor (β2AR)[b] (Class A)	2RH1	TM1–TM1	A loose interface in the extracellular side of TM1	3 × 1 μs CG	The dimer adopts a TM1–TM2–H8 orientation	TM1–TM2–H8
Dimers with intermediate cholesterol molecules						
Human mGluR1 Metabotropic glutamate receptor (Class C)[e]	4OR2	TM1–TM2	cholesterol molecules are stacked between the protomers in the upper bilayer leaflet	3 × 10 μs CG w. original cholesterol 3 × 10 μs CG w/o cholesterol 3 × 10 μs CG in 9:1 POPC: cholesterol	Increased contacts for the TM1–TM2 interface; partial H8–H8 contacts; cholesterol molecules leave the interface	TM1–TM2–H8
Human β2 adrenergic receptor (β2AR)[b,e] (Class A)	2RH1	TM1–H8	Loose TM1–H8 contacts; cholesterol molecules are stacked between the protomers in the lower bilayer leaflet	3 × 10 μs CG w. original cholesterol 3 × 10 μs CG w/o cholesterol 3 × 10 μs CG in 9:1 POPC: cholesterol	The dimer adopts a TM1–TM2–H8 orientation different to the others; original cholesterol molecules leave the interface;	Alt. TM1–TM2–H8

[a] Dimers are also represented by PDB entries 2I36 and 2I37 for Rhodopsin, 3DQB, 4A4 M and 3PXO for activated Rhodopsin/Metarhodopsin II/Opsin, 5C1 M for μOR TM1–TM2–H8, 3NYA for Squid Rhodopsin, 3OE6, 3OE8 & 3OE9 for CXCR4

[b] Biological assemblies, as generated with PDBePISA

[c] Receptor classification based on the Kolakowski A–F system

[d] Number and length of different simulations. CG, Coarse-Grained

[e] The simulations were performed in the presence of original cholesterol molecules, in the absence of any cholesterol and in a 9:1 POPC: cholesterol membrane

Table 2 Overview of simulated theoretical models of GPCR homodimers, including a brief description of the initial dimer interfaces and the changes observed during simulation

Receptor	Original dimer interface	Notes on the initial structure	Number of simulations[a]	Changes after simulation	Final dimer interface
AFM/Cryo-EM Bovine Rhodopsin (Class A)	TM4–TM5	Inferred from AFM/Cryo-EM restraints; More loose interface compared to other TM4–TM5 dimers	3 × 1 μs CG	The inter-protomer distance is reduced	TM4–TM5
AFM/Cryo-EM Bovine Rhodopsin (Class A)	TM1–TM1	Inferred from AFM/Cryo-EM restraints; A loose interface in the extracellular side of TM1	3 × 1 μs CG	The dimer adopts a TM1–TM2–H8 orientation	TM1–TM2–H8
Human mGluR1 Metabotropic glutamate receptor (Class C)	TM4–TM3	TM4–TM4 contacts; This dimer has been classified as energetically weak	3 × 1 μs CG	The dimer adopts a TM4–TM5 interface similar to crystallographic dimers; Cross-linking restraints are satisfied	TM4–TM5
Human δ opioid receptor (δOR) (Class A)	TM4–TM3	TM4–TM4 contacts; This dimer has been classified as energetically weak	3 × 1 μs CG	The dimer adopts a TM4–TM5 interface similar to crystallographic dimers; Cross-linking restraints are satisfied	TM4–TM5
Mouse μ opioid receptor (μOR) (Class A)	TM4–TM3	TM4–TM4 contacts; This dimer has been classified as energetically weak	3 × 1 μs CG	The dimer adopts a TM4–TM5 interface similar to crystallographic dimers; Previous modeling and experimental restraints are satisfied	TM4–TM5

CG Coarse-Grained

[a] Number and length of different simulations

elastic network was applied to protein backbone particles, and secondary structure elements were defined using restraints derived from secondary structure calculations with DSSP [54]. Details on the properties of the network constraints are given in the Supplementary Material, available online. The system was solvated using the standard MARTINI water and ion model, with a salt concentration of 0.15 M NaCl. Each system was subjected to energy minimization, followed by equilibration over 8 ns with gradually decreasing restraints on the protein particles to let the membrane and solvent relax around the proteins. Subsequently, each system was simulated without any restraints, using a 20 fs time step. The properties of each simulation system are presented in Tables 1 and 2 and Supplementary Table S1. All CG-MD simulations were performed using GROMACS v. 4.5.7 [55].

Reverse coarse-graining and all-atom molecular dynamics simulations

The lowest energy frame from the last nanosecond in each CG-MD simulation was used for the reconstruction of atomistic protein models. The group of atoms in each initial all-atom system corresponding to a protein CG particle was translated to the simulation results, such that the center of mass of the group was on the CG particle's final position [56, 57]. The Backward method was applied to reconstruct all-atom representations, using a geometric projection algorithm for reverse Coarse-Graining, followed by a position restrained, force field-based relaxation refinement [58]. This treatment relaxed the unphysical bonds while keeping the overall structure and interactions of the simulated systems intact. Backmapping simulations were performed using GROMACS, the Backward pipeline and the CHARMM36 force field for proteins and lipids [59–61].

A number of subsequent all-atom simulations were performed, to further refine the all-atom models produced by Backward. In cases when it was required, the peptide bond geometry was optimized and localized, biased MD simulations [62] were used to strengthen the integrity of the helical segments, by steering the backbone atoms towards their original secondary structure for short (0.5–2 ns) times. Afterwards, the dimers were re-inserted into an explicit POPC bilayer and, after a number of initial equilibration stages with gradually decreasing restraints, were subjected to a simulated annealing refinement with no position restraints. All-atom simulations were performed using NAMD v. 2.10 [63] and the CHARMM36 force field [59–61]. Detailed information on the simulation protocols can be found in the Supplementary Material, available online. All simulation results and models were analyzed using various GROMACS utilities and analysis scripts

[64], VMD and the Carma suite for structural dynamics analysis [65]. Visualization and plots were built with VMD and the Matplotlib module [66].

Interface analysis and classification

Protein–protein and protein-lipid interactions for CG-MD results were defined using a distance cut-off of 7.5 Å between particles, based on the properties of the MARTINI force field [49, 50]. An additional, time dependent analysis was performed for the change in the Buried Surface Area (BSA) during simulation, calculated as the difference between the Accessible Surface Area (ASA) values of the complex and the isolated protomers. All Coarse-Grained surface calculations were performed using the GROMACS implementation of the Double Cube Lattice algorithm [67] and a 5.2 Å probe radius, based on the properties of the MARTINI water model.

For the initial crystal structures and the final all-atom representations, surface calculations were performed using a 1.4 Å probe radius and DSSP [54] for the calculations. Interface residues for the starting structures as well as the all-atom representations of the final dimer models were further classified as parts of the core or the rim of the BSA, using the Levy classification system [68]. The Relative Accessible Surface Area (RSA) of each residue was calculated as its absolute ASA value, normalized by the maximum ASA value for this residue, as measured in extended Gly-x-Gly tripeptides [69, 70]. Interface residues with RSA < 25 % in the complex and RSA > 25 % in the unbound state were recognized as interface core residues, while residues with RSA > 25 % both in the complex and in the unbound chains were assigned to the rim [68]. An additional interface classification was performed through computational alanine scanning (Ala-scan) mutagenesis. The process involves substitution of each interface residue to alanine, followed by estimation of the change in interaction energy as a result of the mutation ($\Delta\Delta G$). Residues with a $\Delta\Delta G$ value above a specified cut-off are considered as potential Ala-scan hot spots. Alanine scanning was performed with FoldX v. 3.0b6 [71, 72] for protein–protein interactions, using a 1.5 kcal/mol cut-off for the identification of hot spots, while protein-heteroatom interactions were analyzed using the ABS-Scan web server for protein–ligand alanine scanning [73], with a cut-off value of 0.5 kcal/mol.

Dynamical network analysis

The results of the CG-MD simulations were used for the construction and analysis of dynamic networks. Dynamical network analysis applies concepts from network theory to the study of biomolecular structures, by visualizing a structure as a network defined by nodes connected by edges where the nodes represent atoms or molecules, while the edges are the non-bonded interactions. Additional information is provided by the results of Molecular Dynamics simulations, used to weigh the importance of interactions in the network as well as the clustering of network elements through community analysis.

In this work, the procedure originally developed by *Sethi and co-workers* [74] was adapted, slightly modified to accommodate the nature of Coarse-Grained simulations. The last 100 ns of each CG-MD simulation were used as input for network preparation and analysis. Each CG amino acid was represented by a single node, centered at its backbone particle. Protein–protein contacts were defined using the appropriate for MARTINI CG representations distance cut-off. Edges were defined to connect pairs of nodes if the corresponding elements were in contact for more than 75 % of the analyzed trajectory [74]. Covalently bonded residues and nearest neighbors were not considered to be in contact, as they lead to a number of trivial sub-optimal paths in the dynamical network; these also included cysteine pairs forming disulfide bonds, as well as all elastic network restraints used in CG-MD simulations. The weight (w_{ij}) of an edge between nodes i and j was derived from the appropriate pairwise correlation value (C_{ij}) calculated as the normalized covariance for the MD trajectory. Covariance calculations were performed through Cartesian Principal Component Analysis (PCA), and the results were subsequently used to derive the edge weights, with the weight value defined as $w_{ij} = -\log(C_{ij})$.

The physical network of nodes and edges contains substructures of nodes or communities that are more densely interconnected to each other than to other network elements. In the concept of Molecular Dynamics, these network communities define structural elements which move in concert with each other. The optimum community structure is found by maximizing the modularity value (Q), which is a measure of difference in probability of intra- and inter- community edges. Q can have a maximum value of 1; large values of Q indicate better community structure. The shortest paths between pairs of nodes belonging to 2 different communities are calculated and analyzed for communication across communities in the network. Of these intercommunity links, all edges connecting any two of these communities are identified. Edges with the greatest betweenness are pinpointed, and the nodes connected by these edges are established as critical for communication between the structural elements represented by these communities [75]. Trajectory analysis, network preparations and visualization were performed with a slightly modified version of the NetworkView plugin in VMD [53], designed for Dynamical Network Analysis. Correlation (normalized covariance) calculations were performed

through PCA using Carma [65]. Community analysis was performed with the Girvan-Newmann algorithm [75], using the Luthey-Schulten Network Tools [74].

Additional methods

Additional information on Molecular Dynamics simulations and dynamical network analysis can be found in the Supplementary Material, available on line.

Results and discussion

Structural features and diversity in crystallographic GPCR homodimers

A number of structures involving parallel homodimers are available for various GPCRs, featuring symmetric interfaces belonging to the TM1–TM2–H8, TM4–TM5 and TM5–TM6 dimerization types (Fig. 1). Although the overall orientation between different receptor dimers of the same type is generally similar, several features show significant diversity between different receptors and even between dimers of the same receptor. Based on characteristics like the extent of the Buried Surface Area (BSA) and the presence or absence of intermediate hereroatoms, the available crystallographic evidence on GPCR dimer interfaces may be divided into three main categories. Receptor dimers may appear as closely packed interfaces, featuring extensive contacts between the protomers, as loosely packed interfaces, featuring a similar orientation as the closely packed dimers but with a significantly smaller interface and as dimers which, in addition to protein–protein contacts, involve intermediate cholesterol molecules between the protomers (Table 1).

Closely packed homodimers involving the TM1–TM2–H8 interface have been crystallized for bovine Rhodopsin, both in its ground—state form [76] and the ligand—free Opsin intermediate [77], the κ opioid receptor (κOR) [11] and the first of the two different interfaces found in the crystals of μ opioid (μOR) [10] and β1 adrenergic (β1AR) receptors [78]. The structures of κOR and μOR dimers involve fusions with T4 Lysozyme in the protomers' cytoplasmic sides; however, no contacts between the T4L subunits are observed in the TM1–TM2–H8 dimers. Despite the similar orientation of the dimers, significant differences can be observed. An important factor of discrimination between the TM1–TM2–H8 dimers is the relative orientation of each protomer with respect to the other. While in the β1AR and κOR dimers the two protomers are almost parallel to each other and would be expected to sit perpendicular to a membrane plane, in other cases the protomers' principal axes are offset by an angle up to 20°. Characteristic examples include the Rhodopsin and Opsin TM1–TM2–H8 dimers; the different angle of the protomers in these two structures leads to formation of different protein–protein contacts in the two structures. It should be noted that electron crystallography and Cryo-EM experiments for Rhodopsin have shown the protomers adopting a parallel orientation [33, 36]. As such, it can be hypothesized that this angle between the protomers possibly occurred due to the lack of a suitable membrane analogue during crystallization. Another feature of variability observed is the orientation of the TM1 helix, which protrudes away from the helix bundle in the κOR and β1AR but is closer to TM2 in other structures. These differences in orientation essentially lead to a significant diversity in the observed TM1–TM2–H8 dimers.

TM4–TM5 dimers are observed in the structures of squid Rhodopsin [79], the A2A adenosine receptor [80] and the ligand—free β1AR, as well as the class F Smoothened receptor. Cytochrome b562 subunits replace the N-terminal domains but do not form interactions with each other in the Smoothened structure. Similarly, the T4L subunits in the A2A structure do not come into any contact. Therefore, these dimers are unlikely to have been influenced by the presence of these fusions. A model of oligomerized Rhodopsin, based on experimental restraints derived from AFM and Cryo-EM data [31, 32] also displays a TM4–TM5 interface, bearing significant resemblance to the β1AR dimer. Although the extent of the interface differs among structures, all TM4–TM5 dimers display a similar orientation, involving contacts in the transmembrane regions as well as the intracellular ICL2 loop, with some dimers also displaying contacts with the cytoplasmic side of TM3. However, the interprotomer distance is larger in the cases of β1AR, A2A and the AFM Rhodopsin model, while the Smoothened and Squid Rhodopsin structures form more closely packed dimers.

Available TM5–TM6 dimer structures include the second, more prominent dimer interface in the μOR structure, as well as two different interfaces for the CXCR4 chemokine receptor [81]. The μOR dimer consists of extensive contacts between the TM5 and TM6 helices from each protomer that form a transmembrane four helical bundle. Another TM5–TM6 interface is observed for the It1t–bound CXCR4 receptor, however, this dimer involves almost exclusively residues in the extracellular side of the receptors, with very few contacts in the cytoplasmic end of TM5. Furthermore, a variant dimer is formed in the CVX15–bound CXCR4 crystal structure, involving the same interface on the extracellular side but with extensive contacts involving TM4 and the ICL2 loop on the cytoplasmic side. Thus, this interface seems to appear as an intermediate between a TM4–TM5 and a TM5–TM6

dimer. It is important to note that in all three afore mentioned structures T4 Lysozyme constructs have been fused in the place of the ICL3 loop connecting the TM5 and TM6 helices and that in the μOR and It1t-bound CXCR4 dimers the two T4L subunits form contacts with each other, although the degree in which T4L participates in the interface varies. As such, it is unclear whether the TM5–TM6 dimer orientation has been influenced by the presence of the T4L fusions.

Apart from the closely packed interfaces referenced above, a number of loosely packed interfaces exist for some GPCRs. The high resolution crystal structure of the β2 adrenergic receptor (β2AR) [6] features a parallel homodimer involving a few contacts between the TM1 helix extracellular ends. The AFM-based model of oligomerized Rhodopsin also displays a dimer with almost identical orientation to β2AR, as part of a Rhodopsin oligomer that features multiple dimer interfaces (Supplementary Fig. S1). Interestingly, loosely packed TM1–TM1 interfaces have been observed in self-assembly Molecular Dynamics simulations of β1AR and β2AR oligomers [82]. It is possible that this interface could be the precursor to the formation of a more tightly packed TM1–TM2–H8 dimer. A different loose interface is observed in the Squid Rhodopsin structure, involving small contacts in the cytoplasmic side of TM5. However, whether this interface could be a precursor to a TM4–TM5 or a TM5–TM6 dimer is unknown.

Finally, two GPCR structures present parallel homodimers which involve cholesterol molecules. These include a second interface for β2AR, as well as the recently solved mGluR1 metabotropic glutamate receptor transmembrane structure [16]. In both cases the receptors adopt orientations resembling a TM1–TM2–H8 dimer. It should be noted that both GPCRs have been solved as chimeric constructs with T4 Lysozyme (β2AR) and cytochrome b562 (mGluR1). While β2AR shows no contacts between the Lysozymes, a small portion of the BSA in mGluR1 is formed by cytochrome subunits, located at the extracellular side, substituting the large Venus Fly-trap domains (VFD) of Class C GPCRs. A number of protein–protein contacts are observed in both structures, however, a major part of the interface is formed by cholesterol molecules that stack against each other between the protomers, forming a sterol "bridge" that seems to mediate the dimer through protein-cholesterol and cholesterol–cholesterol interactions. The extent of observed protein–protein, protein-cholesterol and cholesterol–cholesterol intermolecular contacts differs between the two structures; the β2AR dimer involves less protein–protein interactions and seems to rely more on adjacent cholesterol molecules than mGluR1, which presents more extensive protein–protein interactions.

Stability and dynamics of GPCR homodimers

Examination of the available structural data reveals that, even though GPCRs seem to form similar dimer interfaces, a significant diversity is observed in the configuration of the protein–protein interfaces. To some extent, this diversity can be attributed to each receptor's distinct structural characteristics. However, several aspects of the interfaces seem to have been influenced by the structure determination process. In order to examine these potential influences and estimate the overall stability and dynamics of GPCR homodimers, each interface was subjected to Molecular Dynamics simulations.

A total of 21 different CG systems were considered for simulation. These dimers were inserted in lipid bilayers and simulated with the MARTINI force field (Supplementary Figure S1). Details for each simulation system are reported in Tables 1 and 2 and Supplementary Table S1. To establish a common time scale for performing simulations, a series of 10 μs long simulations were performed for three selected case studies, namely, the κOR TM1–TM2–H8 dimer, the CXCR4 dimer and the μOR TM5–TM6 dimer. In all cases, structural rearrangements occur very early in the simulations, with the Root Mean Square Deviation (RMSD) of each protein system reaching a plateau within the first 500–1000 ns and remaining relatively stable for the remainder of the simulations (Supplementary Figure S2). Shorter, 1 μs long simulations for the same systems showed a similar dynamic behavior, with all structural changes occurring in the same time scale as the 10 μs runs. Convergence for each system was evaluated by measuring RMSD from the starting conformation as well as the change in the dimers' Buried Surface Area, as measured with a probe adopting the properties of the MARTINI solvent; the analysis showed that the 1 μs time scale is adequate for observing the stabilization of the different dimer interfaces to a stable orientation (Supplementary Figures S3–S7). As a result, all CG-MD systems were simulated for 1 μs, with each simulation replicated in triplicate for validation; an exception was made for all simulations of systems involving cholesterol, which were extended to 10 μs to obtain better sampling for cholesterol movements and interactions (Supplementary Figure S6). The total simulation time accumulates to approximately 270 μs for the Coarse-Grained systems. The lowest energy representations of the final CG-MD conformations were subsequently used for the reconstruction of atomistic representations, using a reverse Coarse-Graining procedure followed by refinement simulations and these models were further used in interface analysis.

It is important to note that none of the simulations that were performed resulted in the dissociation of a dimer interface into its protomers; this included both the 1 μs

long simulations conducted for all dimers and the 10 μs runs conducted for the case studies and cholesterol-associated dimers. However, this observation is in good agreement with what is already known regarding the stability of GPCR dimers and oligomers during simulation. A wide range of self-assembly simulations for several receptors [34, 36, 38, 51, 82] have shown that, even though GPCRs may undergo several early binding and unbinding events before stable assemblies are formed, eventually the simulation systems result in dimers and oligomers that mostly resemble crystallographic dimers such as TM1–TM2–H8 and TM4–TM5, and that remain stable for the remainder of the simulation time, even in simulations conducted in the sub-millisecond scale. In fact, biased Molecular Dynamics and Umbrella Sampling simulations for various dimer interfaces of Rhodopsin [36], β2AR [40], μOR and κOR [83] have shown that known crystallographic TM1–TM2–H8, TM4–TM5 and TM5–TM6 interfaces are characterized by deep energy wells that would be expected to preclude dissociation in the time scales achieved by unbiased Molecular Dynamics simulations. In agreement with these simulations, kinetic analysis derived from Umbrella Sampling simulations for different dimers in β1AR and β2AR have shown that strong dimers, such as the TM1–TM2–H8 interface have an estimated lifetime in the scale of seconds or even minutes, while even weaker interfaces such as TM4–TM4 have an estimated lifetime of milliseconds to seconds [40]. Taken together, all these observations suggest that a complete and accurate description of spontaneous association and dissociation events in GPCR oligomerization may not be achieved by MD simulations, even in cases where simplified models are utilized.

In all simulations the overall GPCR 7TM fold remains stable, with most major fluctuations observed mainly for the loop regions. This is reflected in the RMSD measurements, which range between the values of 5–7 Å when the entirety of the protein particles are included in the calculations, but are in the ranges of 3–4 Å when only the helical segments are considered. These differences can be attributed to the nature of the elastic network used for the Coarse-Grained systems, which applies harmonic restraints to the transmembrane helical fold but not the loop region. Although such a network structure may lead to increased RMSD values, it minimizes the bias to the stoichiometry of the dimer, which has been suggested to be significant when strict elastic restraints are applied to the loops [83].

With a few notable exceptions, explored in greater detail in the following sections, the overall stoichiometry of the crystallographic dimer interfaces remained the same, indicating that the known crystallographic dimers are stable entities. Furthermore, simulations of alternative interfaces for a number of putative dimers for the μOR, δOR and mGluR1 receptors resulted in rearrangements for the assemblies, which adopted features very similar to the crystallographic interfaces, as will be described. These observations are in good agreement with spontaneous self-assembly and Umbrella Sampling simulations for different dimer interfaces in Rhodopsin [36], which have indicated that symmetric dimers resembling those produced by crystal structures are among the most stable oligomerization interfaces, while other, alternative interfaces, even in cases when they meet experimental evidence, are significantly weaker.

However, the observed RMSD values for each dimer were higher than the RMSDs observed for its individual protomers in almost all cases (Fig. 2a, see also Supplementary Table S1). These observations suggest that the main contributions to movements observed during simulation come from rearrangements in the orientation of the interfaces rather than alteration in the structure of the protomers themselves. Even in cases where the overall dimer stoichiometry does not change, these rearrangements lead to the formation of novel protein–protein interactions missing from the original structures; interestingly, several of these novel putative contacts have been identified as parts of GPCR dimer interfaces by several experimental evidence, such as cross-linking and synthetic peptide studies, as it will be outlined. Overall, these results suggest that the orientation of the protomers in the original crystal structures may not be optimal in all cases but that at least some aspects of these crystallographic interfaces could be considered artifacts produced by the applied structure determination processes.

Structural and dynamic behavior of closely packed dimers

The closely packed TM1–TM2–H8 dimers do not display significant deviations, retaining most contacts observed in the original interfaces. Among the different dimers of the dataset, the Rhodopsin, Opsin and μOR dimers displayed the most profound movements regarding the orientation of the protomers, where an angle between the receptors' principal axes is observed. In all three cases this angle is reduced, enabling the formation of more extensive contacts involving residues in the TM1 helix (Fig. 2b). New contacts also involve residues in the first extracellular loop (ECL1) as well as the extracellular end of TM2. The μOR dimer also displays the formation of more extensive contacts in the H8 helix, closely resembling the ones in κOR, while the H8–H8 interface in the Rhodopsin and Opsin dimers resembles more the one in the β1AR dimer. On the other hand, the κOR and β1AR TM1–TM2–H8 dimers display very few changes, retaining their initial configuration. It is important to note that the κOR interface has

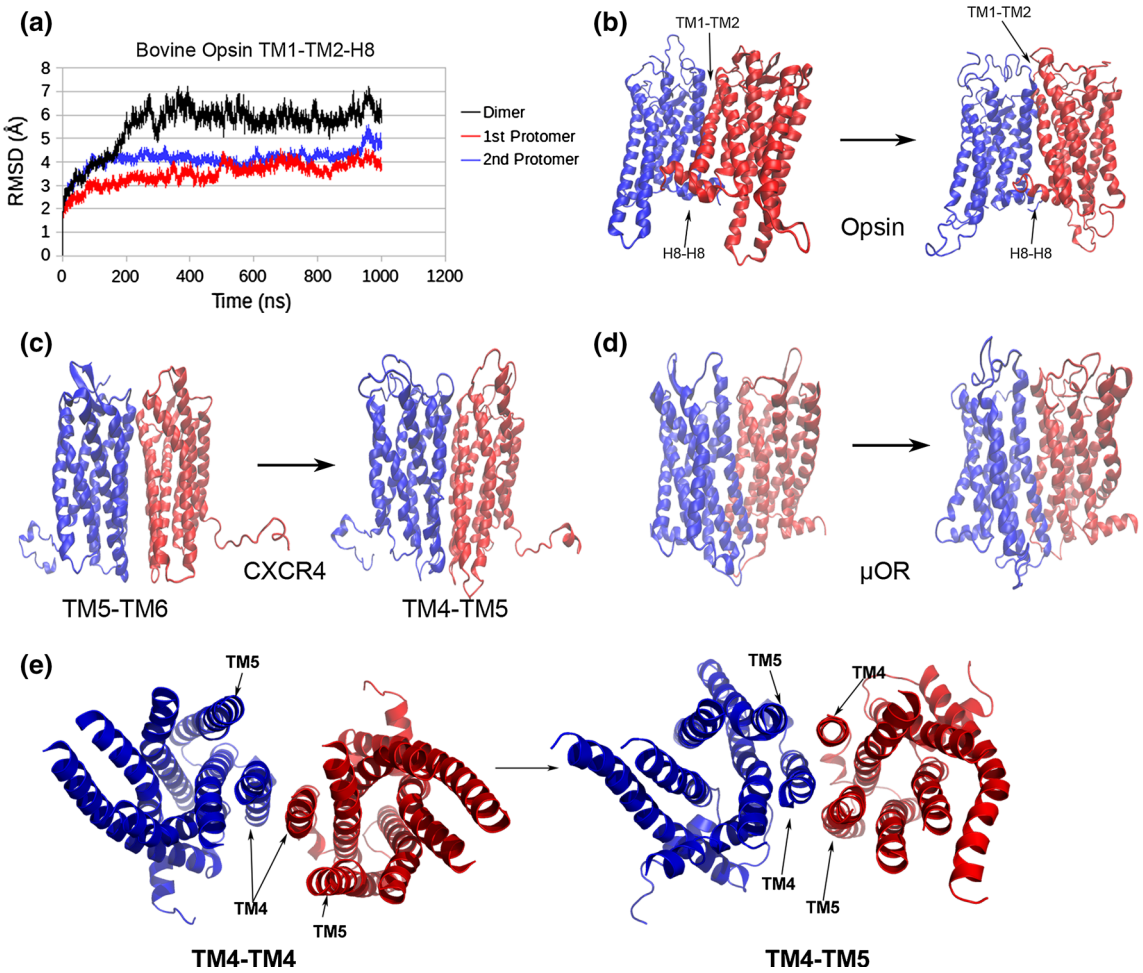

Fig. 2 Examples of results from GPCR homodimer simulations. **a** Time—dependent Root Mean Square Deviaton (RMSD) measurement for the Opsin TM1–TM2–H8 dimer CG-MD simulation. RMSD has been measured with respect to the starting conformation, using the coordinates of the blackbone particles. The *horizontal axis* displays time (in ns), while the *vertical axis* displays RMSD (in Å). All protein segments are considered, including both the transmembrane segments and the interhelical loops. The RMSD of the entire dimer is *colored black*, while the RMSDs of the isolated protomers are *colored blue* and *red*, respectively. **b**, **d** Initial (*left*) and final conformations of the Opsin (**b**), CXCR4 (**c**) and μOR TM5–TM6 (**d**) interfaces. **e** Initial (*left*) and final (*right*) conformations of the alternative dimer interface for δOR. The dimer starts as a TM4–TM4 interface and, during simulation, shifts to a TM4–TM5 interface with features similar to those of crystallographic TM4–TM5 dimers. All structures are shown in cartoon representation, with different protomers *colored blue* and *red*. Initial conformations are represented by the starting crystal structures, while final conformations are represented by all-atom reconstructions of the CG-MD results

been found to fit well to available Cryo-EM volume data for the Metarhodopsin I dimer [33, 36], displaying better correlation in comparison to the Rhodopsin and Opsin original crystallographic interfaces. Overall, these observations suggest that the receptor orientation found in the original κOR structure and proposed by the results of the CG-MD simulations may be more favorable than the original TM1–TM2–H8 structures.

The TM4–TM5 dimers also preserve their overall orientation, with the β1AR and A2A adenosine receptor dimers showing the most profound changes, while the Smoothened dimer remains largely unchanged, with most significant movements observed, as expected, in the extracellular and cytoplasmic regions. All TM4–TM5 dimer simulations result in an almost identical configuration, resembling the one observed in the Smoothened crystal structure. These involve more extensive contacts in TM4 and TM5 and formation of new contacts, formed by residues in the ICL2 loop and the cytoplasmic end of TM3. It is important to note that the latter involves residues in the area of the D(E)RY motif and the TM3–TM6 ionic lock, an important feature of Class A GPCRs that is involved in the process of GPCR activation. The motif seems to form part of the dimer interface in all Class A TM4–TM5 dimer simulations. Interestingly, similar contacts are observed both in the original structure and the simulation result of

Smoothened, although the latter lacks the D(E)RY motif. However, a closer examination of the available Smoothened receptor structures reveals a tight network of contacts between TM3 and TM6 in each protomer, involving residues that are conserved among Class F GPCRs that may serve the same purpose as the TM3–TM6 ionic lock of the D(E)RY motif of Class A receptors [12].

In contrast to the above, significant deviations are observed for some of the TM5–TM6 dimers, in which the original structures contained T4 Lysozyme fusions in close proximity. This is particularly true for the two simulated CXCR4 dimers in the absence of the T4L constructs, which display significant movements. Simulations for both CXCR4 dimers give very similar results. The protomers come closer to each other, forming contacts using residues in transmembrane helices TM4 and TM5 and the second intracellular loop (ICL2), while most TM6 contacts from the original interface dissociate, with the exception of a few interactions involving residues in the second extracellular loop (Fig. 2c). Additional contacts involving the cytoplasmic end of TM3 are also observed. The final models bear a striking resemblance to the other TM4–TM5 dimers. Geometry analysis reveals that most rearrangements occur during the first 30–50 ns of the simulations; subsequently, both dimers remain relatively stable for the rest of the simulations. It is important to note that these Coarse-Grained results are in good agreement with previously published results from much shorter all-atom simulations of CXCR4 [37, 84]. Furthermore, the formation of a TM4–TM5 dimer for CXCR4 is in agreement with experimental studies involving synthetic peptides, which have shown that CXCR4 forms homodimers using residues in TM4 [85] in living malignant cells. Overall, these observations clearly display the important influence the T4 Lysozyme's presence may have had during the structure determination process.

Contrary to CXCR4, the simulated μOR TM5–TM6 interface displays less extensive changes. This crystallographic dimer also includes T4 Lysozymes forming contacts with each other as well as the receptors, but their contributions to the interface are much smaller, and the majority of the buried surface area is formed by extensive TM5–TM6 contacts from each protomer, that form a transmembrane four helical bundle. As such, the interface remains largely unchanged, with significant movement observed mostly for the cytoplasmic ends of the TM5 helices (Fig. 2d). Considering that the T4 Lysozyme was fused in place of the ICL3 loop connecting TM5 and TM6, the original orientation of these transmembrane segments was probably influenced by the presence of T4L during the structure determination process and, therefore, such movements are to be expected. The overall orientation of the protomers remains unchanged, showing the significant stability of the μOR TM5–TM6 interface. However, it is still difficult to assess the potential influence that the T4 Lysozyme fusions may have had in the packing and orientation of the receptors during crystallization.

Simulation of loosely packed dimers leads to closely packed interfaces

Significant structural movements are observed in all simulations performed for the loosely packed Squid Rhodopsin TM5–TM5 and β2AR TM1–TM1 crystallographic homodimers (Supplementary Fig. S8). The squid Rhodopsin TM5–TM5 dimer changes its configuration through the slight rotation of each receptor with respect to their vertical axes, leading to the formation of contacts between the TM5 and TM6 helices. These rearrangements are observed within the first 40–60 ns of the simulation, with the dimer being relatively stable afterwards. This new TM5–TM6 interface bears some resemblance to the μOR TM5–TM6 dimer, but the interacting transmembrane helices do not seem to form a helical bundle. This, however, can be attributed to the distinct structural characteristics of squid Rhodopsin, which displays TM5 and TM6 helices with significantly longer intracellular segments adopting very different conformations compared to the ones observed in vertebrate GPCRs.

More extensive rearrangements are observed in the case of the β2AR TM1–TM1 dimer. The distance between the protomers was decreased, eventually leading to the formation of a TM1–TM2–H8 interface. The new dimer is very similar to other closely packed TM1–TM2–H8 interfaces. Combined with observations from self-assembly β2AR simulations [82], this result could suggest a potential mechanism for the formation of TM1–TM2–H8 GPCR dimers, in which two receptors first come in contact using the extracellular ends of their TM1 helices.

Rearrangements of the interfaces in cholesterol-bound mGluR1 and β2AR dimers

A special case needs to be made for the mGluR1 and β2AR simulations, since a considerable part of both dimers' original interface areas is not formed by the receptors themselves but rather by adjacent cholesterol molecules that seem to mediate the formation and stabilization of the assemblies. An abundance of experimental and computational evidence has suggested that the presence and concentration of cholesterol seems to be connected with the ability of many GPCRs to oligomerize, contributing to the formation and stabilization of quaternary structures or the preference of receptors towards specific types of interfaces [38, 86]. In order to evaluate the features of these cholesterol mediated configurations in the framework of the

present study, the mGluR1 and β2AR dimers were simulated in the presence of cholesterol molecules appearing in the original crystal structures. Although major protein movements occurred in the 1 μs time frame used for other GPCR dimers, these simulations were extended to 10 μs, to achieve better sampling for cholesterol.

CG-MD simulations for both systems displayed a similar behavior for the receptors. During the first steps of both simulations the protomers were observed to decrease the distance between them. Interestingly, cholesterol molecules seemed to remain in their original positions between the receptors, despite the fluidity of the membrane (Supplementary Figs. S9 and S10). Cholesterol—receptor contacts were retained, while contacts between the sterols themselves became more extensive. These movements were observed in both dimer simulations, with the β2AR dimer displaying more profound movements compared to mGluR1. The above observations seem to support the idea that cholesterol enhances the movement of the protomers, essentially driving them towards decreasing their distance. Cholesterol molecules remained in place until the two protomers reached a certain distance from each other. This occurs in the first 100 ns for the mGluR1 dimer, with more time required for the β2AR system (120–150 ns), presumably due to the increased inter-protomer separation. Subsequently, both simulations displayed a gradual exchange between cholesterol molecules and adjacent POPC lipids, eventually leading to removal of almost all cholesterol molecules from their original positions between the receptors, allowing the protomers to further decrease the distance between them.

With regards to the configuration of the final dimer interface, both mGluR1 and β2AR simulations resulted in an increase of TM1–TM2 contacts, as well as contacts involving the ECL1 loop. Furthermore, mGluR1 also displays the formation of new contacts in the cytoplasmic ends of TM7, suggesting a potential H8–H8 interface. However, the final configuration of the β2AR dimer differs from the other TM1–TM2–H8 interfaces, with regards to the orientation of the H8 helices. While other crystallographic TM1–TM2–H8 dimers display direct H8–H8 contacts involving the "outward" side of H8, the β2AR dimer shows TM1–H8/TM1–H8 contacts in the "inward" side, that also faces the cytoplasmic end of TM1 (Supplementary Fig. S11). Interestingly, similar configurations of H8–H8 contacts have been observed in self-assembly simulations of both β2AR [51] and Rhodopsin [36], suggesting it is possible that multiple variations may exist for the TM1–TM2–H8 interface.

In order to further assess the possible contribution of cholesterol towards strengthening the interface, additional simulations were performed for these receptors without the original, crystallographic cholesterol molecules; these included a set of 10 μs long simulations in a purely phospholipid bilayer as well as a bilayer with a 9:1 POPC: cholesterol ratio (Supplementary Figures S6, S12 and S13), mimicking the ratio of monoolein: cholesterol that is usually applied during GPCR crystallization [6, 16]. These simulations resulted in dimer orientations similar to the ones produced by the original simulations. However, the two protomers required significantly longer time to decrease the distance between them when no cholesterol was used, as shown by time—dependent measurement of the distance between the two protomers' centers of mass for β2AR (Supplementary Fig. S13). It is important to note that self-assembly simulations for Rhodopsin [36, 49] and β2AR [51] in bilayers composed exclusively by phospholipids have shown that, even in the absence of cholesterol, simulation setups will eventually produce all known dimerization interfaces. Furthermore, cholesterol has been proposed to enhance dimerization for some GPCRs but has no apparent influence in others. These observations would suggest that, although important, cholesterol is not a prerequisite for the formation of known dimer interfaces. On the other hand, simulations of β2AR featuring different levels of cholesterol in the membrane have shown that cholesterol may influence the stabilization of specific dimer interfaces by interacting with specific binding sites on the receptors [38], suggesting that even though dimer formation may occur in the absence of cholesterol, the presence of the latter in the membrane may help guide the process. Interestingly, these simulations have also shown that cholesterol may enhance the speed of dimer association in some cases. Our results are in agreement with these observations, suggesting that the presence of cholesterol may accelerate the formation of GPCR dimers.

It should be noted that, in both systems, not all cholesterol molecules leave the dimer interface. Instead, cholesterol molecules appear at the rim of the dimer interface, acting as intermediates between the protomers. Furthermore, some of the original cholesterol molecules relocated to different binding sites upon the receptors, including the cleft formed by TM2 and TM4 in both the mGluR1 and β2AR simulations and the lower leaflet side of TM4 in β2AR (Supplementary Fig. S12a). To further investigate the behavior of these putative cholesterol binding sites, we performed evaluations for the distribution of cholesterol in the 9:1 POPC: cholesterol simulations by measuring its partial mass density and distribution around the proteins. Impressively, cholesterol displayed a significant preference for these regions, validating the observations from the simulations featuring only the original cholesterol molecules of the crystal structures (Supplementary Figure S12b). Interestingly, these potential cholesterol binding sites have also been proposed by all-atom and Coarse-Grained simulations for a number of Class A GPCRs

[38, 86] and the observations from the mGluR1 simulation suggest that similar binding sites may exist in receptors from other Classes as well. In fact, some of these sites have been implicated in regulating dimer formation. For example, a highly occupied cholesterol binding site is located in the TM4 helix of β2AR. This site has been proposed to regulate the participation of TM4 in dimer formation during β2AR simulations [38]. Furthermore, experimental studies on protein-cholesterol interactions have also shown that the presence of cholesterol in that region may influence receptor oligomerization in μOR [87]. Although different GPCRs are expected to interact with cholesterol in a different manner, it could be speculated that the presence of cholesterol in that site could have an impact in the formation of TM4–TM5 inter-protomer contacts in general. However, it should be noted that the simulation setups for these systems may not be adequate to capture the dynamics of protein-cholesterol and lipid-cholesterol interactions accurately. The main limitation is the lack of adequate sampling of binding/unbinding events for all observed interaction sites, which would require significantly larger simulation times that are outside the scope of the present study. In the absence of sampling, at least some of the measured properties are expected to be biased. As such, although the results produced by our simulations on GPCR-cholesterol interactions are interesting, they should be interpreted with great care.

Simulations of theoretical dimer models reproduce known crystallographic interfaces

In addition to the crystallographic dimers, CG-MD simulations were performed for a number of theoretical dimer models. These included additional models for Rhodopsin, based on restraints derived from biophysical evidence as well as putative dimers for mGluR1, δOR and μOR, featuring an alternative dimer interface not appearing in crystal structures. As with the crystal structures of the dataset, these theoretical models were also subjected to Coarse-Grained Molecular Dynamics simulations, reverse Coarse-Graining and refinement. The additional Rhodopsin systems involved primarily two dimer interfaces obtained from the model of oligomerized Rhodopsin, based on restraints derived from Atomic Force Microscopy (AFM) and Cryo-EM experiments [31, 32]. These dimers feature a closely packed TM4–TM5 interface, bearing significant resemblance to β1AR and A2A dimers and a loosely packed TM1–TM1 interface, very similar to the loose TM1–TM1 dimer from the β2AR crystal structure. As expected, the CG-MD simulations of these models produced very similar results to the ones reported by CG-MD simulations of the crystallographic dimers. Specifically, the TM4–TM5 model of AFM Rhodopsin displayed the same behavior as the β1AR crystallographic TM4–TM5 dimer, by forming more extensive interactions in TM4 and TM5 and new contacts involving the ICL2 loop and the cytoplasmic end of TM3. Interestingly, residues in the D(E)RY motif also form part of the interface, as it is observed for the crystallographic dimers. Similarly, the loose TM1–TM1 model of AFM Rhodopsin proceeded in forming a closely packed TM1–TM2–H8 interface with features akin to crystallographic Rhodopsin TM1–TM2–H8 dimers, in the same manner as the β2AR TM1–TM1 simulation (Figure S8a).

Special attention must be given to the alternative dimer interfaces that were investigated for mGluR1, δOR and μOR. Experimental evidence, involving cross-linking [28, 43] and mutagenesis studies [87] and computational studies including molecular modeling and correlated mutation analysis [88] have proposed that these receptors may use residues in TM4 to form their homo- and heterodimer interfaces. Although restraints defined by such studies can be satisfied by TM4–TM5 dimers produced by crystal structures, other, alternative assemblies can be proposed, including a putative dimer interface featuring symmetric contacts involving mainly the TM4 helix and a part of TM3, henceforth mentioned as TM4–TM4, instead of a TM4–TM5 interface. However, its stability has been found to be questionable. Specifically, Umbrella Sampling simulations have shown that, compared to crystallographic dimers such as TM1–TM2–H8 or TM4–TM5, a TM4–TM4 dimer would be significantly weaker and have classified the interface as transient [36, 40]. In agreement with these simulations, a scoring-based docking assay has recently shown that a dimer involving TM4 and TM3 is favorable only when TM5 is also part of the interface [89]. Finally, additional experimental evidence has proposed potential interface contacts involving the TM5 helix along with TM4 [43]. Taken together, these studies would propose that the stoichiometry of a dimer satisfying such experimental restraints would be a TM4–TM5 interface rather than TM4–TM4.

To further test this hypothesis in the framework of the current study, we modeled putative TM4–TM4 dimers for the δOR, μOR and mGluR1 receptors. The models were constructed in a manner that restricted all protein–protein contacts to the TM4 and TM3 helices, excluding TM5, while at the same time satisfying experimental restraints about interface residues in TM4. The models were subsequently subjected to CG-MD simulations for 1 μs, during which significant rearrangements of the orientation of the protomers were observed. Specifically, in all three cases the protomers rotated with respect to one another, leading to the formation of contacts between residues in TM4 and TM5 and essentially resulting in TM4–TM5 interfaces very similar to the β1AR crystallographic dimer (Fig. 2e).

Impressively, these new assemblies satisfied all original experimental restraints for TM4, as well as restraints for interface residues in TM5, providing further mitigation towards their validity. As such, our results from these simulations show that the TM4–TM5 assemblies proposed by crystallographic evidence, compared to other putative dimers, are preferable entities.

Apart from shifts in the interface, the newTM4–TM5 dimers present novel features that were also observed during the simulation of crystallographic TM4–TM5 dimers, including the formation of contacts with the cytoplasmic end of TM3. In both δOR and μOR receptors, belonging to Class A these contacts included regions around the D(E)RY motif participating in the ionic lock between TM3 and TM6, as it was in the case of the crystallographic interfaces. Interestingly, similar contacts were observed for the mGluR1 TM4–TM5 dimer, belonging to Class C. Although Class C GPCRs lack the D(E)RY motif, the recent crystal structures of mGluR1 and mGluR5 have shown the existence of a similar ionic lock between charged residues in TM3 (R3.53 in the B&W numbering) and TM6 (E6.35 in the B&W numbering) that are conserved among Class C GPCRs and have been proposed as the equivalent of the Class A feature [15, 16].

Contribution of polar and aromatic contacts near the membrane boundaries

Interface analysis was conducted on both the original crystal structures and simulation results, using a surface area definition accompanied by classification of interacting residues based on surface burial. A relative ASA (RSA) term was used, taking into account the differences in size and properties for each amino acid side chain to identify residues as parts of the Buried Surface Area's core or rim. Interface analysis reveals that most core residues are located in the TM1 helix of TM1–TM2–H8 dimers and TM5 of the various TM5 dimers. To a lesser extent, some core residues also appear in the TM4 and H8 areas. Not surprisingly, hydrophobic interactions form the majority of the interface. However, a significant presence of polar and charged residues is also observed. In most cases, these polar residues seem to interact with other similar groups, with a few hydrogen bonds also observed, formed with other polar or charged groups, elements of the backbone or, in some cases, the –OH group of a tyrosine side chain.

With regards to hydrophobic interactions, approximately 9–30 % of each dimer's BSA includes aromatic residues. A more detailed interatomic contacts analysis reveals that a significant number of these aromatic residues form π-stacking interactions, while aromatic-Proline and aromatic-amino group contacts are also observed. Further classification of interacting residues was attempted using computational alanine scanning mutagenesis, a process that involves substitution of each interface residue to alanine, followed by estimation of the change in binding energy upon mutation. Core residues and Ala-scan hot spots seem to be in good agreement and the overall surface of the Ala-scan hot spots overlaps with the interface core (Fig. 3). More importantly, the most prominent hot spots in almost all cases include intermolecular hydrogen bonds and aromatic residues participating in π-stacking interactions. All identified interface hot spots are included in Supplementary Table S2.

The extent to which these hot spots appear in the interface differs among dimers. Several stacking interactions and polar contacts are observed in the κOR and CXCR4 dimers and a complex π-stacking network is observed in the class F Smoothened TM4–TM5 dimer (Supplementary Fig. S14). Stacking pairs and hydrogen bonds are also formed in the ground-state Rhodopsin and Opsin TM1–TM2–H8 dimers. The TM4–TM5 dimers in the Rhodopsin AFM model and the A2A and Squid Rhodopsin structures also have some aromatic stacking pairs. On the other hand, the μOR TM1–TM2–H8 dimer shows no such hot spots in its original crystallographic structure, possibly due to its differences in orientation with κOR and other TM1–TM2–H8 dimers, as already described. These differences also affect the Rhodopsin and Opsin dimers, which display hot spots in different regions. The β1AR TM4–TM5 and μOR TM5–TM6 also show very few aromatic interactions but, instead, have an increased number of polar contacts.

Impressively, some of the most profound hot spots that were identified through this analysis involved residues that have been experimentally found to contribute to GPCR dimer interfaces (see underlined residues in Supplementary Table S2). Examples include stacking interactions involving W175 and Y206, which are located in transmembrane segments TM4 and TM5 of Rhodopsin, respectively. Impressively, those same residues have been identified as parts of a dimer interface in Rhodopsin though cross-linking experiments [90]. Similarly, C316 was also identified as a hot spot in all Rhodopsin TM1–TM2–H8 dimers after simulation, again, in agreement with cross-linking. However, it should be noted that no such contacts were observed in the starting conformation of the dimers, suggesting that rearrangements are required for the original interfaces to be in agreement with experimental evidence. Such hot spots were also observed for the simulated TM4–TM5 dimer models of μOR, δOR and mGluR1, again, in agreement with cross-linking evidence for these receptors.

It is important to note that for all simulated dimers, stacking interactions and hydrogen bonds that were classified as core residues or Ala-scan hot spots in the initial structures were retained throughout the simulations.

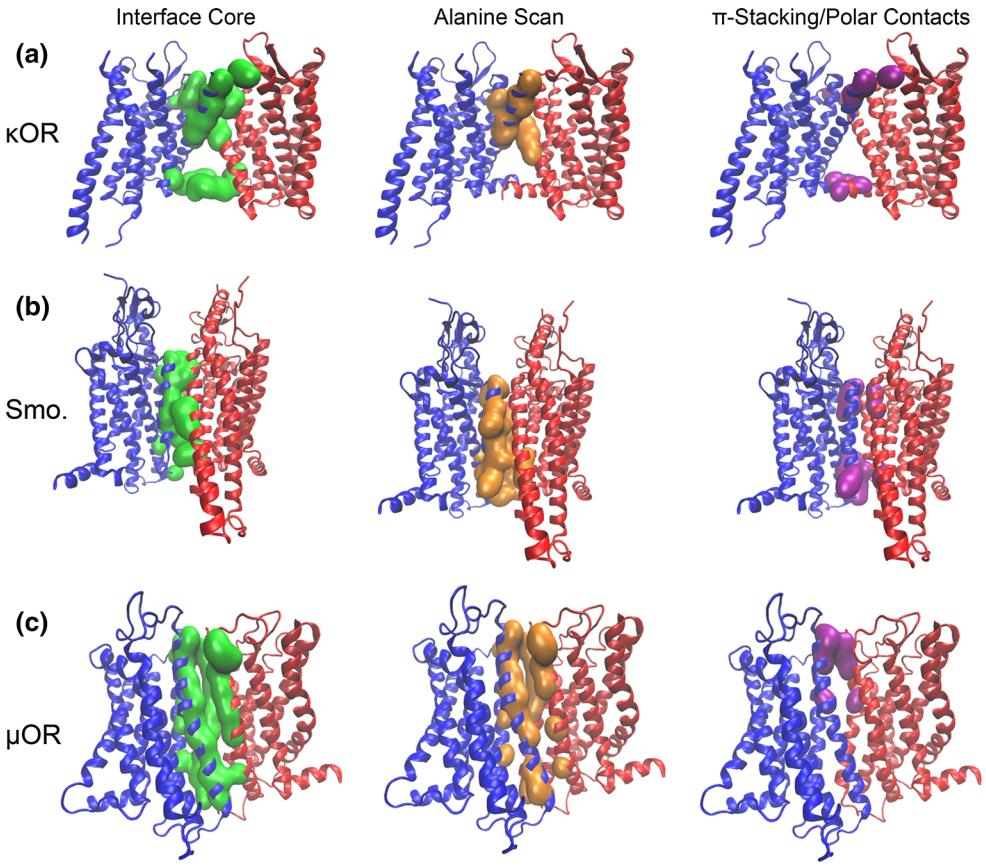

Fig. 3 Examples of interface classification, Ala-scan hot spots and aromatic stacking interactions for the κOR TM1–TM2–H8 (**a**), Smoothened TM4–TM5 (**b**) and μOR TM5–TM6 (**c**) dimers. Receptors are shown in cartoon orientation, with different protomers *colored blue* and *red*. Interface core residues, hot spots and stacking pairs are shown in isosurface representation and *colored green*, *orange* and *purple*, respectively

Furthermore, in dimers where extensive structural movements were reported, new contacts also included a significant amount of π-stacking interactions, which were formed during the early stages and were retained for the remainder of the simulations (Supplementary Table S2). Interesting cases include the μOR TM1–TM2–H8 dimer which, after assuming its new configuration, displays the formation of multiple stacking interactions resembling the ones observed in κOR, as well as the Rhodopsin and Opsin dimers, which resulted in dimers with seemingly identical stacking pairs. Impressively, the TM1–TM2–H8 interface formed by the loosely packed TM1–TM1 dimer also showed interactions in the same regions. Subsequent interface analysis and Ala-scan calculations showed that these new stacking interactions were also classified as core residues and Ala-scan hot spots.

An interesting case of hot spots appears in the mGluR1 and β2AR dimers with adjacent cholesterol molecules. Protein-cholesterol contact residues in mGluR1 include, among others, W588 and F646 from each protomer, which form stacking—like interactions with the ring segments of adjacent cholesterol molecules. Similar interactions are observed between cholesterol molecules and F49 from each protomer in the β2AR—cholesterol dimer. A protein—ligand Ala-scan trial on the initial structures shows that these aromatic residues contribute the most to cholesterol binding, displaying the highest ΔΔG values. As already described, protein—cholesterol contacts are retained for a large part of the mGluR1 and β2AR CG-MD simulations. Interestingly, after the departure of cholesterol from the mGluR1 dimer interface, these protein—cholesterol hot spots participate in stacking interactions that are classified as protein–protein interface hot spots, very similar to those observed in other GPCR dimers (Supplementary Table S2).

With a few notable exceptions, such as the hydrogen bond formed between Ser residues in the μOR and κOR TM1–TM2–H8 dimers (a residue that appears to be conserved in the opioid receptor subfamily), most stacking and polar interactions are located primarily near the cytoplasmic and extracellular ends of the transmembrane helices TM1, TM4 and TM5, as well as the C-terminal H8 helix

(Fig. 3), meaning that these hot spots are mainly located near the membrane boundaries. Impressively, cross-linking experiments aimed at studying the dimer interfaces of various GPCRs, including mammalian Class A GPCRs such as Rhodopsin [90], D2 dopamine [26] and δOR [28], the Class D Ste2 pheromone receptor in yeast [27] and, more recently, the Class C metabotropic glutamate receptor subfamily [43], have implicated residues in these positions as potential protein–protein interface hot spots. Furthermore, recent experiments involving synthetic peptides and mass spectrometry have shown that oligomerization in Rhodopsin can be disrupted by blocking regions near the membrane boundaries of TM1, TM2 and TM4 [91]. Results from our analysis are in good agreement with these studies, indicating that the significant contributions of residues near the membrane boundaries can be a common feature in several GPCR dimers.

In monomeric GPCRs, residues in such positions could lead to unalleviated hydrophobic mismatch due to difference between the length of the transmembrane segments and the membrane's hydrophobic thickness, resulting to high energy costs due to unfavorable exposure of nonpolar residues to the solvent or polar and charged residues to the lipid bilayer's hydrophobic core. It has been suggested that the energetics of residual hydrophobic mismatch can be an important factor in the aggregation of transmembrane proteins, leading to the formation of protein–protein interactions as a means to alleviate the high energy penalty of the mismatch [92]. Furthermore, Coarse-Grained Molecular Dynamics simulations have proposed that phospholipids with different lipid tail lengths may display different behavior patterns with regards to hydrophobic mismatch, eventually affecting the aggregation rate in the oligomerization of Rhodopsin in model membranes [34]. The close proximity of the strongest hot spots to the membrane boundaries in GPCR dimers, as proposed by the current study, could be a result of this phenomenon and a further indication towards a role for the membrane as a structural determinant in the spatial organization of GPCRs.

Network properties and community organization of GPCR dimers

The dynamics of GPCR dimers, as described by the performed simulation, were further evaluated through the construction and analysis of dynamical networks. The last 100 ns of each CG-MD simulation were used to prepare dynamical networks (Supplementary Table S3) for all studied GPCR dimers. In the networks constructed, each residue of the simulated dimers was represented as a node of the network. Any two non neighboring nodes are connected by an edge if they are in contact for the majority (>75 %) of the analyzed simulation, i.e. if the distance between them is less than a defined cutoff. Individual edges may have associated weights or lengths based on properties such as correlated motions, energies or physical distance. Edges between nodes are weighted by correlation values obtained from PCA calculations for the simulation, so that the distance between the two nodes reduces as the correlation (or energy of interaction) between the monomers increases. In this sense, edges with the lowest weight values represent the most correlated and, therefore, strongest residue–residue contacts in the network.

A path between two nodes is simply a set of nodes and edges connecting one node to the other, and the path length is the sum of weights for edges in the path. Multiple paths may exist between two nodes. If there are multiple communication paths nearly equal in length, then not all residues along these paths need be considered as important. Instead, only residues or interactions that occur in the highest number of suboptimal pathways need to be conserved to guarantee an effective pathway for communication in the complex. Instead, for two nodes within a connected network, there exists at least one optimal, shortest path between them, and slightly longer paths are referred to as suboptimal.

These paths are considered to be crucial for network communication, representing interatomic contacts that play an important role in the dynamics of the studied structure. A time-averaged, dynamic study of the network's connectivity may utilize these characteristics to identify the substructure of communities into the network. Network communities are defined as a sum of nodes belonging to the same subnetwork, that are more densely interconnected to one another compared to nodes outside this community and can communicate with each other relatively easy through multiple routes. These communities, which can contain both amino acids and nucleotides, are thought to be similar to domains, but are defined by the dynamics of the biomolecules. As such, from a structural viewpoint, these communities can represent parts of the proteins that move in concert with each other. Two different communities can often be in contact or overlapping, with nodes belonging to both clusters. Communication across these groups is estimated by identifying the shortest paths between these intercommunity nodes. Such edges are defined as critical, representing contacts that may prove to be important for communication between two structural segments.

Interestingly, all networks presented a modularity score (Q) in the area of 0.7–0.8 (Supplementary Table S3), displaying an optimal community structure and nearing the values often found in real-world networks [75]. Although these communities may not necessarily correspond to structural features, a number of motion correlations with potential structural significance are reported. More

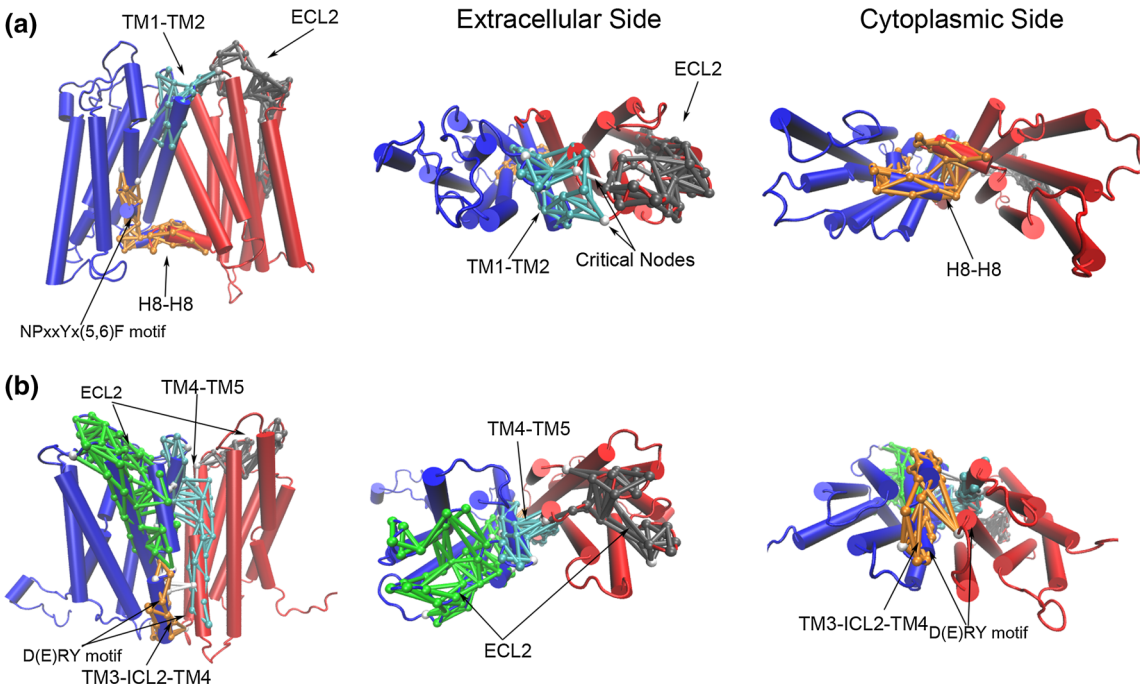

Fig. 4 Inter-protomer and Extracellular Loop 2 (ECL2) network communities for the κOR TM1–TM2–H8 (**a**) and CXCR4 TM4–TM5 (**b**) dynamic networks. Side, extracellular and cytoplasmic views are shown. Receptors are *corored blue* and *red*, with helical segments shown as cylinders. Network elements are represented with spheres for nodes and sticks for edges and different communities are depicted using distinct colors. Critical connections (nodes and edges) between communities are colored white. Dimer interfaces and other important GPCR features are labeled accordingly. Full network representations, with all communities, are shown for these structures in Supplementary Figures S8 and S9

importantly, a conserved appearance of specific communities is observed, revealing possible common features in GPCR structure and dynamics, as well as dimer interactions.

Specifically, simulated TM1–TM2–H8 dimers display the formation of a community containing the dimer interface of the TM1 and TM2 helices (Fig. 4a, see also Supplementary Fig. S15). Such a community is reported for all Class A receptor dimers, including the new AFM Rhodopsin and β2AR assemblies formed during their respective simulations. A second dimerization community appearing in some of the TM1–TM2–H8 simulations is formed by the cytoplasmic ends of TM7 and the H8 helices, containing not only the H8–H8 interface but also the conserved NPxxYx(5,6)F motif (Fig. 4a), present in both Class A and Class C GPCRs. Specifically, such communities are reported for the Rhodopsin, κOR and μOR dimers and, surprisingly, a similar community is observed in the case of mGluR1, despite the lack of complete coordinates for the H8 helices. Finally, although not directly involved with dimerization, community structures containing the ECL2 loop are observed for both protomers in all simulations, in which the ECL2 loops are either part of the TM1–TM2/TM1–TM2 community themselves or are connected with it through critical nodes and edges (Supplementary Fig. S15).

Although not as extensive as the one reported for the TM1–TM2–H8 dimers, a similar conservation of network features is observed for TM4–TM5 dimers (Fig. 4b, see also Supplementary Fig. S16). In each case two inter-protomer communities are formed, one containing part of the dimer interface area between TM4 and TM5 and the other containing the interface between the ICL2 loops and the cytoplasmic ends of TM3; the latter contains the D(E)RY areas, which also participate in inter—protomer contacts (Fig. 4b). The only exception to these rules is the β1AR TM4–TM5 dimer, in which no TM4–TM5 community is observed. This can be partially attributed to the overall interface of the β1AR dimer, which is considerably loosely packed compared to other TM4–TM5 dimers, even after the simulations. Interestingly, this particular dimer contains the least amount of stacking/polar interactions among TM4–TM5 dimers. Similar to the TM1–TM2–H8 dimers, communities containing the ECL2 loop and, depending on its presence, residues from the N-terminus are formed, connected to inter—protomer communities through critical nodes and edges. In fact, in some instances, these communities also contain residues of TM4 and TM5,

participating in dimerization interactions. Such communities are observed not only for the Class A receptors but also for the Class F Smoothened and Class C mGluR1 TM4–TM5 dimers. Furthermore, they are also observed for the two dimers of CXCR4 that resulted during simulation, providing further support to the notion that CXCR4 adopts features of a TM4–TM5 dimer rather than TM5–TM6 (Supplementary Fig. S16).

In contrast to the above cases, the μOR TM5–TM6 dimer stands out, in the sense that none of the previously mentioned features are observed. Communities are formed containing the TM1 and TM2 helices as well as the TM6 and TM7 helices, suggesting a co—dependent movement of these transmembrane segments. Small communities are also observed involving the D(E)RY motif and residues in TM5 and TM6, but without any inter—protomer contacts involved. Instead, almost all significant inter—protomer contacts are modeled as critical nodes connecting the otherwise independent communities of each protomer. Interestingly, part of the TM5–TM6 dimer interface forms a community with the ECL2 loop in each receptor protomer. While these results are interesting, the lack of other available crystallographic TM5–TM6 dimers hinders any attempt to detect any conserved features, since the CXCR4 dimers shifted to a TM4–TM5 orientation during simulation. However, it should be noted that the simulated TM5–TM6 dimer for squid Rhodopsin shows an almost identical community network organization (Supplementary Fig. S17).

The presence and similarity of these network elements in the simulated dimers suggest a conserved nature in GPCR structure and dynamic behavior. Furthermore, the observation of inter—protomer communities displays the dense interconnectivity of these regions, suggesting the considerable strength of inter—protomer contacts in these regions. A comparison of the dimers' network structure with results obtained through Alanine scanning and interface analysis reveals that the location of these communities overlaps with regions rich in interface core residues and Ala-scan hot spots (Figs. 3, 4). Finally, it should be noted that all stable stacking interactions, observed through interface analysis, appear to be part of these inter—protomer communities.

Conserved features in GPCR homodimer interfaces

Overall, the proposed Molecular Dynamics, interface analysis and community network results suggest the presence of conserved structural features in TM1–TM2–H8, TM4–TM5 and TM5–TM6 GPCR dimers, despite the often low sequence similarity between the receptors. It is important to note that the final orientation of all dimers appears to be relatively stable for more than half the simulation time in each system, suggesting favorable thermodynamic properties for these configurations. Interestingly, the Class C mGluR1 and Class F Smoothened dimers display significant structural and dynamic similarities with Class A GPCR dimers. It should be noted that all Smoothened and mGluR1 simulations were both performed using only the transmembrane segments of the receptors, making it impossible to ascertain the possible influence of their large extracellular domains. These influences can be of great importance, especially in the case of metabotropic glutamate receptors, for which a significant amount of evidence shows that the extracellular Venus Fly-trap domains form part of the dimer interface [93]. However, the proposed results, combined with the significant structural similarity of the transmembrane α-helical bundle between these receptors and other GPCRs suggests that the observed oligomerization features may be common for all GPCR classes.

Structural and dynamic insights on the functional impact of GPCR dimers

A pivotal aspect in GPCR oligomerization research is studying the possible implications of oligomeric interactions upon receptor function. In numerous occasions, GPCR dimers and oligomers have been reported to influence or be influenced by ligand binding, regulate receptor activation and G-protein binding or initiate internalization and the β-arrestin signaling path [18]. However, despite the abundance of experimental evidence, little is known concerning the structural nature of these influences.

Regarding GPCR activation, a number of crystal structures for activated receptors in various stages have become available, including various Rhodopsin intermediates [76, 77] and the β2AR-G-protein complex [94]. GPCRs in all of these structures display the same structural patterns for activation, which include breaking the ionic lock formed between TM6 and the D(E)RY motif in TM3, followed by movements of the TM5 and TM6 cytoplasmic segments and the ICL3 loop, with some minor rearrangements in the TM3 helix also observed. This motif is a common feature in all Class A receptors. GPCRs from other classes, including the Class C mGluR1 and Class F Smoothened receptors, lack this feature. However, a similar ionic lock has been observed in the recently solved mGluR1 and mGluR5 structures [15, 16] and a tight network of interactions between TM3 and TM6 exists in the Smoothened structure. A second motif, NPxxYx(5,6)F that in the cytoplasmic end of TM7 is also implicated in the process, seemingly stabilizing the active state by forming contacts with TM6. The significant similarity of these features in all activated GPCR structures, as well as the high conservation of the above mentioned motifs among

the members of class A suggests that the pattern of these movements is highly conserved in Rhodopsin—like GPCRs. Furthermore, the observation of a potential ionic lock between TM3 and TM6 in recently solved Class B and C structures, as well as the existence of variations for the NPxxYx(5,6)F motif in non Class A receptors [13–16] could be indications that other GPCRs may follow a similar activation process.

As expected, these structural rearrangements appear in the structure of the Opsin dimer. Furthermore, structural alignment of an activated receptor to any TM1–TM2–H8 dimer shows no potential clashes between the receptor's active state and the dimer interface (Supplementary Figure S18). Considering that no regions participating in activation are actually part of the TM1–TM2–H8 interface, the above observation is not surprising. In any case, it is clear that a TM1–TM2–H8 dimer can allow receptor activation and, consequently, canonical GPCR signal transduction. Similarly, Opsin and the adenosine bound active A2A adenosine receptor can be aligned to their respective TM4–TM5 dimers without introducing any bumps. It can be surmised, therefore, that the TM4–TM5 dimer may also allow GPCR activation, although participation of residues in the TM3 and TM5 helices to the dimer interface could affect the activation process. On the other hand, alignment of an active GPCR to the μ opioid TM5–TM6 interface displays serious clashes, due to the orientation of the TM5 and TM6 helices in the dimer. These clashes are observed both for the original μOR structure and for the result of the CG-MD simulation. The above observations indicate the inability of the receptors in such a dimer towards proper activation (Supplementary Figure S18). Considering that there is experimental evidence implicating opioid receptor heterodimerization with inhibitory mechanisms, the hypothesis that a TM5–TM6 dimer could be a part of an inhibitory process could be viable.

An evaluation through structural alignment such as the one described provides hints towards each dimerization type's ability to shift to the active GPCR state, but offers little towards unveiling more detailed information regarding how the TM1–TM2–H8 and TM4–TM5 dimers may regulate the process. However, the study of simulation results through network analysis and community clustering shows correlations between elements of the dimer interface and regions implicated in activation that may be part of these regulatory mechanisms. Specifically, all the Class A GPCR TM4–TM5 dimer networks display the formation of inter—protomer communities including the region of the D(E)RY motif, the ICL2 loop and TM4 from each protomer, suggesting that these segments move in concert during simulation (Fig. 4b, see also Supplementary Figure S16). Surprisingly, a similar community is observed for the Smoothened and mGluR1 TM4–TM5 dimers even though they lack the motif; however, the similar packing of the TM3 and TM6 helices in Smoothened and the existence of an ionic lock in mGluR1 would suggest that these receptors may be activated in a similar manner. A second correlation between elements of the activation process and dimerization is also observed for the μOR, κOR, Rhodopsin, β2AR and mGluR1 TM1–TM2–H8 interfaces, which display the formation of communities involving the H8 helices and parts of the TM7 helix, including the NPxxYx(5,6)F motif, with the dense connectivity of these community elements hinting towards regulation of the motif by the H8–H8 interface (Fig. 4a). These correlations of motions between these regions and the dimer interfaces suggests that the dynamic behavior of these motifs and, possibly, their participation in the activation process by stabilizing the inactive or active state, could be subject to influences from the presence of a second receptor protomer.

The collective study of ligand binding mechanisms in GPCRs is challenging, both due to the presence of multiple binding sites on the same receptor and due to the significant diversity of GPCR ligands, which range from small molecules to large peptides and steroid hormones. Despite these limitations, a number of GPCR structures with various antagonists, synthetic or even native agonists have become available, including some receptors appearing in GPCR dimers. Furthermore, experimental evidence has implicated the contribution of the second extracellular loop (ECL2) to ligand recognition and selectivity for a number of different GPCRs [95].

Combining the information regarding the binding sites of these ligands with structural information, results from Molecular Dynamics and the dimers' network properties can propose possible mechanisms for the relationship between oligomerization and ligand recognition. Regarding the relations between GPCR oligomerization and the various ligand binding sites, it should be noted that many of the available dimer interfaces contain regions that also form part of ligand binding sites. The CXCR4 chemokine receptor is a characteristic example, with its TM4–TM5 interface overlapping with the It1t, CVX15 and vMIP-II binding pockets. Similarly, the adenosine site in A2A overlaps with its TM4–TM5 dimer, while the carvedilol and carazolol interacting residues are in close proximity to the dimer interfaces of β1AR and β2AR, respectively (Supplementary Figure S19). Finally, network analysis displays correlation between the dimer interfaces and the protomers' ECL2 loops, with the latter being either a direct part of an inter—protomer community or connected to one through critical nodes and edges (Fig. 4, see also Supplementary Figures S8–S10). It should be noted that a different network approach, combining structural features and co-evolution information, has suggested an evolutionary

correlation between ECL2 and a TM4–TM5 interface obtained through all-atom MD simulations for CXCR4 [84]. Our results, based solely on structural and dynamic GPCR features examined through Coarse-Grained Molecular Dynamics are in good agreement with these observations, since a similar correlation is observed. In fact, correlations between ECL2 and the dimer interface are reported in all examined dimerization interfaces, suggesting the possible connection between the interfaces and a GPCR region implicated in ligand recognition and selectivity, as well as hinting towards the existence of potential mechanisms through which TM1–TM2–H8, TM4–TM5 and TM5–TM6 dimers may regulate, or be regulated by ligand recognition.

Limitations of the model and methodology

It is important to state some of the limitations underlying the proposed models and the methodology used. With regards to the applied methodology, an important limitation may be the choice of using a Coarse-Grained force field to model biomolecular interactions. Our simulations with the MARTINI force field have shown good agreement with atomistic simulations for specific case studies and, more importantly, experimental evidence on the nature of the dimer interfaces. Still, the chosen model results in a loss of detail that limits the accurate representation of intermolecular contacts. A second limitation may be the poor sampling of membrane properties, particularly in the cases of simulations involving cholesterol. While the chosen simulation setups may describe the dynamic behavior of protein–protein interactions adequately, they fail to capture the membrane's slow dynamics, such as the phospholipid and cholesterol diffusion or measuring the stability of protein-cholesterol interactions. Adequate sampling for these phenomena would require significantly larger simulation times that are outside the scope of the present study. As such, any observations regarding these properties should be interpreted with care.

Regarding the methods used for intermolecular contacts analysis, it should be noted that both surface-based classification of the interface and computational alanine scanning have been developed with soluble proteins in mind and have not been extensively validated against transmembrane proteins. However, the good agreement between simulation results and interface analysis suggests that both methods can be used in transmembrane protein–protein interactions.

Finally, it should be noted that the present study focuses solely on symmetric dimer interfaces featuring TM1, TM4 and TM5, mainly due to their increased observation in crystal structures, biochemical evidence and Molecular Dynamics simulations. However, a few GPCR structures [32, 81, 96] and a number of self-assembly Molecular Dynamics simulations have also proposed the potential formation of dimers involving different regions or even non-symmetric dimers, either as a result of specific environmental conditions such as membrane composition [38] or as a means through which more than two receptors may interact to form higher order oligomers [36, 39, 82]. While the strength of these alternative dimer interfaces has been challenged by free-energy calculations [36], the potential structural and physiological relevance or irrelevance of these assemblies warrants further investigation. Furthermore, the current study offers very little towards unveiling the nature of protein–protein interactions in GPCR hetero-oligomerization, although it should be noted that both the available evidence and the conserved structural nature of the GPCR transmembrane bundle would suggest that GPCR heteromers may display similar features as GPCR homomers. Despite these limitations, the results proposed by this study reveal important aspects of the structural nature in GPCR oligomerization.

Conclusions

In this study we explored aspects of the structural nature and dynamic behavior of GPCR dimer interactions. Molecular Dynamics simulations showed structural movements that can occur in GPCR dimers, suggesting possible rearrangements of the observed crystallographic interfaces. Additionally, the contribution of inter—protomer aromatic interactions and polar contacts near the membrane boundaries was explored, hinting at the existence of potential interface hot spots in GPCR oligomeric interactions as well as the potential role of the membrane, which may act as a structural determinant in driving the formation of dimer interactions in GPCRs. Finally, potential aspects of the influence dimer formation may have upon GPCR function were highlighted and possible regions of interest for the study of regulatory mechanisms were proposed. To our knowledge, this is one of the first studies to collectively examine the dynamic behavior of the available GPCR oligomerization structural evidence, as well as examine the structural nature of GPCR oligomerization for receptors outside of Class A. Given the rising interest in unveiling the implications of GPCR oligomerization and the significant structural conservation among GPCRs, the results of our study could be applicable in the design of experimental studies involving GPCR dimers and oligomers, as well as the study of transmembrane protein–protein interactions in general.

Acknowledgments We would like to thank the scientific and administrative staff of the "Bioinformatics" Master's Program at the

Faculty of Biology of the University of Athens, for its generous support. M.C.T. was financially supported as a postdoctoral fellow by Greek State Scholarships Foundation, through the Siemens Program: "IKY Fellowships of Excellence for Postgraduate Studies in Greece – Siemens Program (2014–2015)". This work was supported by computational time granted from the Greek Research & Technology Network (GRNET) in the National HPC facility—ARIS under project ID "PR001025-M.D.S.B.M.S.". Finally, we would like to sincerely thank the anonymous reviewers for their very valuable and constructive criticism, which helped us to considerably improve the manuscript, as well as the Editor-in-Chief for properly handling it. The authors declare no conflicts of interest.

References

1. Rosenbaum DM, Rasmussen SG, Kobilka BK (2009) The structure and function of G-protein-coupled receptors. Nature 459(7245):356–363. doi:10.1038/nature08144
2. Cherezov V, Abola E, Stevens RC (2010) Recent progress in the structure determination of GPCRs, a membrane protein family with high potential as pharmaceutical targets. Methods Mol Biol 654:141–168. doi:10.1007/978-1-60761-762-4_8
3. Oldham WM, Hamm HE (2008) Heterotrimeric G protein activation by G-protein-coupled receptors. Nat Rev Mol Cell Biol 9(1):60–71. doi:10.1038/nrm2299
4. Kolakowski LF Jr (1994) GCRDb: a G-protein-coupled receptor database. Recept Channels 2(1):1–7
5. Palczewski K, Kumasaka T, Hori T, Behnke CA, Motoshima H, Fox BA, Le Trong I, Teller DC, Okada T, Stenkamp RE, Yamamoto M, Miyano M (2000) Crystal structure of rhodopsin: a G protein-coupled receptor. Science 289(5480):739–745
6. Cherezov V, Rosenbaum DM, Hanson MA, Rasmussen SG, Thian FS, Kobilka TS, Choi HJ, Kuhn P, Weis WI, Kobilka BK, Stevens RC (2007) High-resolution crystal structure of an engineered human beta2-adrenergic G protein-coupled receptor. Science 318(5854):1258–1265. doi:10.1126/science.1150577
7. Warne T, Serrano-Vega MJ, Baker JG, Moukhametzianov R, Edwards PC, Henderson R, Leslie AG, Tate CG, Schertler GF (2008) Structure of a beta1-adrenergic G-protein-coupled receptor. Nature 454(7203):486–491. doi:10.1038/nature07101
8. Xu F, Wu H, Katritch V, Han GW, Jacobson KA, Gao ZG, Cherezov V, Stevens RC (2011) Structure of an agonist-bound human A2A adenosine receptor. Science 332(6027):322–327. doi:10.1126/science.1202793
9. Granier S, Manglik A, Kruse AC, Kobilka TS, Thian FS, Weis WI, Kobilka BK (2012) Structure of the delta-opioid receptor bound to naltrindole. Nature 485(7398):400–404. doi:10.1038/nature11111
10. Manglik A, Kruse AC, Kobilka TS, Thian FS, Mathiesen JM, Sunahara RK, Pardo L, Weis WI, Kobilka BK, Granier S (2012) Crystal structure of the mu-opioid receptor bound to a morphinan antagonist. Nature 485(7398):321–326. doi:10.1038/nature10954
11. Wu H, Wacker D, Mileni M, Katritch V, Han GW, Vardy E, Liu W, Thompson AA, Huang XP, Carroll FI, Mascarella SW, Westkaemper RB, Mosier PD, Roth BL, Cherezov V, Stevens RC (2012) Structure of the human kappa-opioid receptor in complex with JDTic. Nature 485(7398):327–332. doi:10.1038/nature10939
12. Wang C, Wu H, Katritch V, Han GW, Huang XP, Liu W, Siu FY, Roth BL, Cherezov V, Stevens RC (2013) Structure of the human smoothened receptor bound to an antitumour agent. Nature 497(7449):338–343. doi:10.1038/nature12167
13. Hollenstein K, Kean J, Bortolato A, Cheng RK, Dore AS, Jazayeri A, Cooke RM, Weir M, Marshall FH (2013) Structure of class B GPCR corticotropin-releasing factor receptor 1. Nature 499(7459):438–443. doi:10.1038/nature12357
14. Siu FY, He M, de Graaf C, Han GW, Yang D, Zhang Z, Zhou C, Xu Q, Wacker D, Joseph JS, Liu W, Lau J, Cherezov V, Katritch V, Wang MW, Stevens RC (2013) Structure of the human glucagon class B G-protein-coupled receptor. Nature 499(7459):444–449. doi:10.1038/nature12393
15. Dore AS, Okrasa K, Patel JC, Serrano-Vega M, Bennett K, Cooke RM, Errey JC, Jazayeri A, Khan S, Tehan B, Weir M, Wiggin GR, Marshall FH (2014) Structure of class C GPCR metabotropic glutamate receptor 5 transmembrane domain. Nature 511(7511):557–562. doi:10.1038/nature13396
16. Wu H, Wang C, Gregory KJ, Han GW, Cho HP, Xia Y, Niswender CM, Katritch V, Meiler J, Cherezov V, Conn PJ, Stevens RC (2014) Structure of a class C GPCR metabotropic glutamate receptor 1 bound to an allosteric modulator. Science 344(6179):58–64. doi:10.1126/science.1249489
17. Ferre S, Casado V, Devi LA, Filizola M, Jockers R, Lohse MJ, Milligan G, Pin JP, Guitart X (2014) G protein-coupled receptor oligomerization revisited: functional and pharmacological perspectives. Pharmacol Rev 66(2):413–434. doi:10.1124/pr.113.008052
18. Franco R, Casado V, Cortes A, Ferrada C, Mallol J, Woods A, Lluis C, Canela EI, Ferre S (2007) Basic concepts in G-protein-coupled receptor homo- and heterodimerization. Sci World J 7:48–57. doi:10.1100/tsw.2007.197
19. Borroto-Escuela DO, Brito I, Romero-Fernandez W, Di Palma M, Oflijan J, Skieterska K, Duchou J, Van Craenenbroeck K, Suarez-Boomgaard D, Rivera A, Guidolin D, Agnati LF, Fuxe K (2014) The G protein-coupled receptor heterodimer network (GPCR-HetNet) and its hub components. Int J Mol Sci 15(5):8570–8590. doi:10.3390/ijms15058570
20. Kniazeff J, Prezeau L, Rondard P, Pin JP, Goudet C (2011) Dimers and beyond: the functional puzzles of class C GPCRs. Pharmacol Ther 130(1):9–25. doi:10.1016/j.pharmthera.2011.01.006
21. Dalrymple MB, Pfleger KD, Eidne KA (2008) G protein-coupled receptor dimers: functional consequences, disease states and drug targets. Pharmacol Ther 118(3):359–371. doi:10.1016/j.pharmthera.2008.03.004
22. Niswender CM, Conn PJ (2010) Metabotropic glutamate receptors: physiology, pharmacology, and disease. Annu Rev Pharmacol Toxicol 50:295–322. doi:10.1146/annurev.pharmtox.011008.145533
23. Lee CW, Ho IK (2013) Pharmacological profiles of oligomerized mu-opioid receptors. Cells 2(4):689–714. doi:10.3390/cells2040689
24. Moreno JL, Holloway T, Gonzalez-Maeso J (2013) G protein-coupled receptor heterocomplexes in neuropsychiatric disorders. Prog Mol Biol Transl Sci 117:187–205. doi:10.1016/B978-0-12-386931-9.00008-8
25. Wade SM, Dalman HM, Yang SZ, Neubig RR (1994) Multisite interactions of receptors and G proteins: enhanced potency of dimeric receptor peptides in modifying G protein function. Mol Pharmacol 45(6):1191–1197
26. Guo W, Shi L, Javitch JA (2003) The fourth transmembrane segment forms the interface of the dopamine D2 receptor homodimer. J Biol Chem 278(7):4385–4388. doi:10.1074/jbc.C200679200
27. Wang HX, Konopka JB (2009) Identification of amino acids at two dimer interface regions of the alpha-factor receptor (Ste2). Biochemistry 48(30):7132–7139. doi:10.1021/bi900424h
28. Johnston JM, Aburi M, Provasi D, Bortolato A, Urizar E, Lambert NA, Javitch JA, Filizola M (2011) Making structural sense of dimerization interfaces of delta opioid receptor homodimers. Biochemistry 50(10):1682–1690. doi:10.1021/bi101474v

29. Kaczor AA, Selent J (2011) Oligomerization of G protein-coupled receptors: biochemical and biophysical methods. Curr Med Chem 18(30):4606–4634
30. Hu J, Thor D, Zhou Y, Liu T, Wang Y, McMillin SM, Mistry R, Challiss RA, Costanzi S, Wess J (2012) Structural aspects of M(3) muscarinic acetylcholine receptor dimer formation and activation. FASEB J 26(2):604–616. doi:10.1096/fj.11-191510
31. Fotiadis D, Liang Y, Filipek S, Saperstein DA, Engel A, Palczewski K (2003) Atomic-force microscopy: rhodopsin dimers in native disc membranes. Nature 421(6919):127–128. doi:10.1038/421127a
32. Liang Y, Fotiadis D, Filipek S, Saperstein DA, Palczewski K, Engel A (2003) Organization of the G protein-coupled receptors rhodopsin and opsin in native membranes. J Biol Chem 278(24):21655–21662. doi:10.1074/jbc.M302536200
33. Ruprecht JJ, Mielke T, Vogel R, Villa C, Schertler GF (2004) Electron crystallography reveals the structure of metarhodopsin I. EMBO J 23(18):3609–3620. doi:10.1038/sj.emboj.7600374
34. Periole X, Huber T, Marrink SJ, Sakmar TP (2007) G protein-coupled receptors self-assemble in dynamics simulations of model bilayers. J Am Chem Soc 129(33):10126–10132. doi:10.1021/ja0706246
35. Simpson LM, Taddese B, Wall ID, Reynolds CA (2010) Bioinformatics and molecular modelling approaches to GPCR oligomerization. Curr Opin Pharmacol 10(1):30–37. doi:10.1016/j.coph.2009.11.001
36. Periole X, Knepp AM, Sakmar TP, Marrink SJ, Huber T (2012) Structural determinants of the supramolecular organization of G protein-coupled receptors in bilayers. J Am Chem Soc 134(26):10959–10965. doi:10.1021/ja303286e
37. Rodriguez D, Gutierrez-de-Teran H (2012) Characterization of the homodimerization interface and functional hotspots of the CXCR4 chemokine receptor. Proteins 80(8):1919–1928. doi:10.1002/prot.24099
38. Prasanna X, Chattopadhyay A, Sengupta D (2014) Cholesterol modulates the dimer interface of the beta(2)-adrenergic receptor via cholesterol occupancy sites. Biophys J 106(6):1290–1300. doi:10.1016/j.bpj.2014.02.002
39. Provasi D, Boz MB, Johnston JM, Filizola M (2015) Preferred supramolecular organization and dimer interfaces of opioid receptors from simulated self-association. PLoS Comput Biol 11(3):e1004148. doi:10.1371/journal.pcbi.1004148
40. Johnston JM, Wang H, Provasi D, Filizola M (2012) Assessing the relative stability of dimer interfaces in g protein-coupled receptors. PLoS Comput Biol 8(8):e1002649. doi:10.1371/journal.pcbi.1002649
41. Berman HM, Westbrook J, Feng Z, Gilliland G, Bhat TN, Weissig H, Shindyalov IN, Bourne PE (2000) The protein data bank. Nucleic Acids Res 28(1):235–242
42. Krissinel E, Henrick K (2007) Inference of macromolecular assemblies from crystalline state. J Mol Biol 372(3):774–797. doi:10.1016/j.jmb.2007.05.022
43. Xue L, Rovira X, Scholler P, Zhao H, Liu J, Pin JP, Rondard P (2015) Major ligand-induced rearrangement of the heptahelical domain interface in a GPCR dimer. Nat Chem Biol 11(2):134–140. doi:10.1038/nchembio.1711
44. Schrödinger, LLC (2010) The PyMOL molecular graphics system, Version 1.7
45. Humphrey W, Dalke A, Schulten K (1996) VMD: visual molecular dynamics. J Mol Graph 14(1):33–38
46. Eswar N, Webb B, Marti-Renom MA, Madhusudhan MS, Eramian D, Shen M-y, Pieper U, Sali A (2001) Comparative protein structure modeling using MODELLER. In: Coligan JE (ed) Current protocols in protein science, Wiley, Hoboken. doi:10.1002/0471140864.ps0209s50
47. Consortium TU (2015) UniProt: a hub for protein information. Nucleic Acids Res 43(D1):D204–D212. doi:10.1093/nar/gku989
48. Larkin MA, Blackshields G, Brown NP, Chenna R, McGettigan PA, McWilliam H, Valentin F, Wallace IM, Wilm A, Lopez R, Thompson JD, Gibson TJ, Higgins DG (2007) Clustal W and Clustal X version 2.0. Bioinformatics 23(21):2947–2948. doi:10.1093/bioinformatics/btm404
49. Marrink SJ, Risselada HJ, Yefimov S, Tieleman DP, de Vries AH (2007) The MARTINI force field: coarse grained model for biomolecular simulations. J Phys Chem B 111(27):7812–7824. doi:10.1021/jp071097f
50. Monticelli L, Kandasamy SK, Periole X, Larson RG, Tieleman DP, Marrink S-J (2008) The MARTINI coarse-grained force field: extension to proteins. J Chem Theory Comput 4(5):819–834. doi:10.1021/ct700324x
51. Ghosh A, Sonavane U, Joshi R (2014) Multiscale modelling to understand the self-assembly mechanism of human beta2-adrenergic receptor in lipid bilayer. Comput Biol Chem 48:29–39. doi:10.1016/j.compbiolchem.2013.11.002
52. Wassenaar TA, Ingólfsson HI, Böckmann RA, Tieleman DP, Marrink SJ (2015) Computational lipidomics with insane: a versatile tool for generating custom membranes for molecular simulations. J Chem Theory Comput 11(5):2144–2155. doi:10.1021/acs.jctc.5b00209
53. Eargle J, Luthey-Schulten Z (2012) NetworkView: 3D display and analysis of protein.RNA interaction networks. Bioinformatics 28(22):3000–3001. doi:10.1093/bioinformatics/bts546
54. Kabsch W, Sander C (1983) Dictionary of protein secondary structure: pattern recognition of hydrogen-bonded and geometrical features. Biopolymers 22(12):2577–2637. doi:10.1002/bip.360221211
55. Pronk S, Pall S, Schulz R, Larsson P, Bjelkmar P, Apostolov R, Shirts MR, Smith JC, Kasson PM, van der Spoel D, Hess B, Lindahl E (2013) GROMACS 4.5: a high-throughput and highly parallel open source molecular simulation toolkit. Bioinformatics 29(7):845–854. doi:10.1093/bioinformatics/btt055
56. Shih AY, Freddolino PL, Arkhipov A, Schulten K (2007) Assembly of lipoprotein particles revealed by coarse-grained molecular dynamics simulations. J Struct Biol 157(3):579–592. doi:10.1016/j.jsb.2006.08.006
57. Shih AY, Freddolino PL, Sligar SG, Schulten K (2007) Disassembly of nanodiscs with cholate. Nano Lett 7(6):1692–1696. doi:10.1021/nl0706906
58. Wassenaar TA, Pluhackova K, Bockmann RA, Marrink SJ, Tieleman DP (2014) Going backward: a flexible geometric approach to reverse transformation from coarse grained to atomistic models. J Chem Theory Comput 10(2):676–690. doi:10.1021/ct400617g
59. Brooks BR, Brooks CL 3rd, Mackerell AD Jr, Nilsson L, Petrella RJ, Roux B, Won Y, Archontis G, Bartels C, Boresch S, Caflisch A, Caves L, Cui Q, Dinner AR, Feig M, Fischer S, Gao J, Hodoscek M, Im W, Kuczera K, Lazaridis T, Ma J, Ovchinnikov V, Paci E, Pastor RW, Post CB, Pu JZ, Schaefer M, Tidor B, Venable RM, Woodcock HL, Wu X, Yang W, York DM, Karplus M (2009) CHARMM: the biomolecular simulation program. J Comput Chem 30(10):1545–1614. doi:10.1002/jcc.21287
60. Lim JB, Rogaski B, Klauda JB (2012) Update of the cholesterol force field parameters in CHARMM. J Phys Chem B 116(1):203–210. doi:10.1021/jp207925m
61. Huang J, MacKerell AD Jr (2013) CHARMM36 all-atom additive protein force field: validation based on comparison to NMR data. J Comput Chem 34(25):2135–2145. doi:10.1002/jcc.23354
62. Schlitter J, Engels M, Kruger P (1994) Targeted molecular dynamics: a new approach for searching pathways of conformational transitions. J Mol Graph 12(2):84–89

63. Phillips JC, Braun R, Wang W, Gumbart J, Tajkhorshid E, Villa E, Chipot C, Skeel RD, Kale L, Schulten K (2005) Scalable molecular dynamics with NAMD. J Comput Chem 26(16):1781–1802. doi:10.1002/jcc.20289
64. Castillo N, Monticelli L, Barnoud J, Tieleman DP (2013) Free energy of WALP23 dimer association in DMPC, DPPC, and DOPC bilayers. Chem Phys Lipids 169:95–105. doi:10.1016/j.chemphyslip.2013.02.001
65. Glykos NM (2006) Software news and updates. Carma: a molecular dynamics analysis program. J Comput Chem 27(14):1765–1768. doi:10.1002/jcc.20482
66. Hunter JD (2007) Matplotlib: a 2D graphics environment. Comput Sci Eng 9(3):90–95
67. Eisenhaber F, Lijnzaad P, Argos P, Sander C, Scharf M (1995) The double cubic lattice method: efficient approaches to numerical integration of surface area and volume and to dot surface contouring of molecular assemblies. J Comput Chem 16(3):273–284. doi:10.1002/jcc.540160303
68. Levy ED (2010) A simple definition of structural regions in proteins and its use in analyzing interface evolution. J Mol Biol 403(4):660–670. doi:10.1016/j.jmb.2010.09.028
69. Chothia C (1976) The nature of the accessible and buried surfaces in proteins. J Mol Biol 105(1):1–12
70. Miller S, Janin J, Lesk AM, Chothia C (1987) Interior and surface of monomeric proteins. J Mol Biol 196(3):641–656
71. Guerois R, Nielsen JE, Serrano L (2002) Predicting changes in the stability of proteins and protein complexes: a study of more than 1000 mutations. J Mol Biol 320(2):369–387. doi:10.1016/S0022-2836(02)00442-4
72. Schymkowitz J, Borg J, Stricher F, Nys R, Rousseau F, Serrano L (2005) The FoldX web server: an online force field. Nucleic Acids Res 33(Web Server issue):W382–W388. doi:10.1093/nar/gki387
73. Anand P, Nagarajan D, Mukherjee S, Chandra N (2014) ABS-Scan: in silico alanine scanning mutagenesis for binding site residues in protein-ligand complex. F1000Research 3:214. doi:10.12688/f1000research.5165.2
74. Sethi A, Eargle J, Black AA, Luthey-Schulten Z (2009) Dynamical networks in tRNA:protein complexes. Proc Natl Acad Sci USA 106(16):6620–6625. doi:10.1073/pnas.0810961106
75. Girvan M, Newman ME (2002) Community structure in social and biological networks. Proc Natl Acad Sci USA 99(12):7821–7826. doi:10.1073/pnas.122653799
76. Salom D, Lodowski DT, Stenkamp RE, Le Trong I, Golczak M, Jastrzebska B, Harris T, Ballesteros JA, Palczewski K (2006) Crystal structure of a photoactivated deprotonated intermediate of rhodopsin. Proc Natl Acad Sci USA 103(44):16123–16128. doi:10.1073/pnas.0608022103
77. Park JH, Scheerer P, Hofmann KP, Choe HW, Ernst OP (2008) Crystal structure of the ligand-free G-protein-coupled receptor opsin. Nature 454(7201):183–187. doi:10.1038/nature07063
78. Huang J, Chen S, Zhang JJ, Huang XY (2013) Crystal structure of oligomeric beta1-adrenergic G protein-coupled receptors in ligand-free basal state. Nat Struct Mol Biol 20(4):419–425. doi:10.1038/nsmb.2504
79. Murakami M, Kouyama T (2008) Crystal structure of squid rhodopsin. Nature 453(7193):363–367. doi:10.1038/nature06925
80. Liu W, Chun E, Thompson AA, Chubukov P, Xu F, Katritch V, Han GW, Roth CB, Heitman LH, IJzerman AP, Cherezov V, Stevens RC (2012) Structural basis for allosteric regulation of GPCRs by sodium ions. Science 337(6091):232–236. doi:10.1126/science.1219218
81. Wu B, Chien EY, Mol CD, Fenalti G, Liu W, Katritch V, Abagyan R, Brooun A, Wells P, Bi FC, Hamel DJ, Kuhn P, Handel TM, Cherezov V, Stevens RC (2010) Structures of the CXCR4 chemokine GPCR with small-molecule and cyclic peptide antagonists. Science 330(6007):1066–1071. doi:10.1126/science.1194396
82. Mondal S, Johnston JM, Wang H, Khelashvili G, Filizola M, Weinstein H (2013) Membrane driven spatial organization of GPCRs. Sci Rep 3:2909. doi:10.1038/srep02909
83. Johnston JM, Filizola M (2014) Differential stability of the crystallographic interfaces of mu- and kappa-opioid receptors. PLoS ONE 9(2):e90694. doi:10.1371/journal.pone.0090694
84. Nichols SE, Hernandez CX, Wang Y, McCammon JA (2013) Structure-based network analysis of an evolved G protein-coupled receptor homodimer interface. Protein Sci Publ Protein Soc 22(6):745–754. doi:10.1002/pro.2258
85. Wang J, He L, Combs CA, Roderiquez G, Norcross MA (2006) Dimerization of CXCR4 in living malignant cells: control of cell migration by a synthetic peptide that reduces homologous CXCR4 interactions. Mol Cancer Ther 5(10):2474–2483. doi:10.1158/1535-7163.MCT-05-0261
86. Cang X, Du Y, Mao Y, Wang Y, Yang H, Jiang H (2013) Mapping the functional binding sites of cholesterol in beta2-adrenergic receptor by long-time molecular dynamics simulations. J Phys Chem B 117(4):1085–1094. doi:10.1021/jp3118192
87. Zheng H, Pearsall EA, Hurst DP, Zhang Y, Chu J, Zhou Y, Reggio PH, Loh HH, Law PY (2012) Palmitoylation and membrane cholesterol stabilize mu-opioid receptor homodimerization and G protein coupling. BMC cell biology 13:6. doi:10.1186/1471-2121-13-6
88. Filizola M, Olmea O, Weinstein H (2002) Prediction of heterodimerization interfaces of G-protein coupled receptors with a new subtractive correlated mutation method. Protein Eng 15(11):881–885
89. Kaczor AA, Guixà-González R, Carrió P, Poso A, Dove S, Pastor M, Selent J (2015) Multi-component protein–protein docking based protocol with external scoring for modeling dimers of G protein-coupled receptors. Mol Inf 34(4):246–255. doi:10.1002/minf.201400088
90. Kota P, Reeves PJ, Rajbhandary UL, Khorana HG (2006) Opsin is present as dimers in COS1 cells: identification of amino acids at the dimeric interface. Proc Natl Acad Sci USA 103(9):3054–3059. doi:10.1073/pnas.0510982103
91. Jastrzebska B, Chen Y, Orban T, Jin H, Hofmann L, Palczewski K (2015) Disruption of rhodopsin dimerization with synthetic peptides targeting an interaction interface. J Biol Chem 290(42):25728–25744. doi:10.1074/jbc.M115.662684
92. Mondal S, Khelashvili G, Weinstein H (2014) Not just an oil slick: how the energetics of protein-membrane interactions impacts the function and organization of transmembrane proteins. Biophys J 106(11):2305–2316. doi:10.1016/j.bpj.2014.04.032
93. Kunishima N, Shimada Y, Tsuji Y, Sato T, Yamamoto M, Kumasaka T, Nakanishi S, Jingami H, Morikawa K (2000) Structural basis of glutamate recognition by a dimeric metabotropic glutamate receptor. Nature 407(6807):971–977. doi:10.1038/35039564
94. Rasmussen SG, DeVree BT, Zou Y, Kruse AC, Chung KY, Kobilka TS, Thian FS, Chae PS, Pardon E, Calinski D, Mathiesen JM, Shah ST, Lyons JA, Caffrey M, Gellman SH, Steyaert J, Skiniotis G, Weis WI, Sunahara RK, Kobilka BK (2011) Crystal structure of the beta2 adrenergic receptor-Gs protein complex. Nature 477(7366):549–555. doi:10.1038/nature10361
95. Seibt BF, Schiedel AC, Thimm D, Hinz S, Sherbiny FF, Muller CE (2013) The second extracellular loop of GPCRs determines subtype-selectivity and controls efficacy as evidenced by loop exchange study at A2 adenosine receptors. Biochem Pharmacol 85(9):1317–1329. doi:10.1016/j.bcp.2013.03.005
96. Tan Q, Zhu Y, Li J, Chen Z, Han GW, Kufareva I, Li T, Ma L, Fenalti G, Zhang W, Xie X, Yang H, Jiang H, Cherezov V, Liu H, Stevens RC, Zhao Q, Wu B (2013) Structure of the CCR5 chemokine receptor-HIV entry inhibitor maraviroc complex. Science 341(6152):1387–1390. doi:10.1126/science.1241475